HHS Public Access

Author manuscript

Mol Microbiol. Author manuscript; available in PMC 2017 August 01.

Published in final edited form as:

Mol Microbiol. 2016 August ; 101(4): 625–644. doi:10.1111/mmi.13414.

Function, expression, specificity, diversity, and incompatibility of actinobacteriophage *parABS* systems

Rebekah M. Dedrick[^], **Travis N. Mavrich**[^], **Wei L. Ng**, **Juan C. Cervantes Reyes**, **Matthew R. Olm**[1], **Rachael E. Rush**, **Deborah Jacobs-Sera**, **Daniel A. Russell**, and **Graham F. Hatfull**[*]

Department of Biological Sciences, University of Pittsburgh, Pittsburgh, PA 15260

Abstract

More than 180 individual phages infecting hosts in the phylum Actinobacteria have been sequenced and grouped into Cluster A because of their similar overall nucleotide sequences and genome architectures. These Cluster A phages are either temperate or derivatives of temperate parents, and most have an integration cassette near the center of the genome containing an integrase gene and *attP*. However, about 20% of the phages lack an integration cassette, which is replaced by a 1.4 kbp segment with predicted partitioning functions, including plasmid-like *parA* and *parB* genes. Phage RedRock forms stable lysogens in *Mycobacterium smegmatis* in which the prophage replicates at 2.4 copies/chromosome and the partitioning system confers prophage maintenance. The *parAB* genes are expressed upon RedRock infection of *M. smegmatis*, but are down-regulated once lysogeny is established by binding of RedRock ParB to *parS-L*, one of two centromere-like sites flanking the *parAB* genes. The RedRock *parS-L* and *parS-R* sites are composed of eight directly repeated copies of an 8 bp motif that is recognized by ParB. The actinobacteriophage *parABS* cassettes span considerable sequence diversity and specificity, providing a suite of tools for use in mycobacterial genetics.

Graphical Abstract

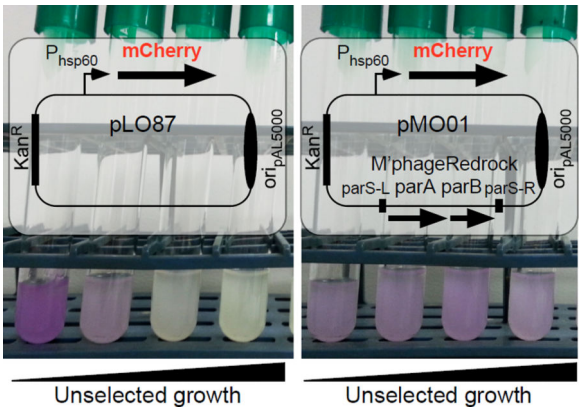

[*]Corresponding author, gfh@pitt.edu.

[^]These authors contributed equally

[1]Current address: Department of Plant and Microbial Biology, University of California, Berkeley, Berkeley, CA 94720

Introduction

A large collection of sequenced actinobacteriophage genomes provides high-resolution insights into their genetic diversity and evolution (Pope *et al.*, 2015). The more than 1,300 sequenced phage genomes (http://phagesdb.org), can be organized into over two-dozen clusters (Cluster A, B, C, etc.) composed of distinct nucleotide sequences, many of which can be divided into subclusters based on their overall sequence similarities. There is substantial diversity within subclusters, and their architecturally mosaic genomes reflect a long evolutionary history of genetic exchange (Hatfull *et al.*, 2010, Pope *et al.*, 2015). The genetic diversity is reflected in considerable biological novelty and these phages have provided numerous insights into gene expression, regulation, and function (Hatfull, 2010, Hatfull, 2012, Hatfull, 2014).

Many of the actinobacteriophages are either temperate, or are recent derivatives of temperate parents (Hatfull, 2014). A majority of the phages encode an integrase of either the tyrosine- or serine- class of site-specific recombinases that mediate prophage formation by chromosomal integration (Hatfull, 2014). Several phages (particularly those organized in Clusters P, N, and I) employ an unusual system of life cycle regulation in which the phage attachment site for integration (*attP*) is located within the repressor gene, such that the 3' end of the repressor that encodes a degradation tag is recombinationally dissociated from the rest of the gene, resulting in repressor stabilization (Broussard *et al.*, 2013). In other phage genomes such as L5 and Bxb1 (both organized in Cluster A), prophage integration is independent of repressor synthesis, although the immunity system is unusual in that the repressor binds to a large number (~25–30) of repressor binding sites distributed across the genomes (Jain & Hatfull, 2000, Brown *et al.*, 1997, Pope *et al.*, 2011). Repressor binding interferes with transcriptional progression and these sites are known as 'stoperators', in contrast to the operator sites that regulate transcription initiation (Brown *et al.*, 1997).

Cluster A is the largest group of actinobacteriophages, and currently can be divided into 17 subclusters (A1 – A17). However, these all share a common organization in which the virion structure and assembly genes are organized with a common synteny in the left arms, and the right arms contain DNA metabolism and regulatory genes, along with a large number of small open reading frames of unknown function [see Fig. 1A, (Hatfull & Sarkis, 1993, Hatfull, 2012)]. The left arm genes are transcribed rightwards, and the right arm genes are typically transcribed leftwards, although some of the phages (primarily within Subcluster A1) also have up to six genes at the right ends of the genomes that are also transcribed rightwards (Hatfull, 2012). Most of the Cluster A phages encode an integrase gene and a closely-linked *attP* site situated at the center of the genomes, between the left and right arm genes (Hatfull, 2012, Hatfull, 2014).

Bacterial chromosomes and many plasmids – especially those replicating at low copy number – encode a partitioning system that enables segregation of plasmid molecules into both daughter cells at division, resulting in stable maintenance of the plasmid in a population of cells (Baxter & Funnell, 2014, Ebersbach & Gerdes, 2005). The partitioning systems are highly diverse but can be organized into three main groups, Type I (subdivided into Ia and Ib), II and III, each of which typically contains a centromere binding protein (CBP), an

ATPase or GTPase partitioning protein, and a centromere-like DNA site (Reyes-Lamothe *et al.*, 2012, Wang *et al.*, 2013, Baxter & Funnell, 2014, Ebersbach & Gerdes, 2005). The CBP binds to the centromere-like site, and the NTPase uses nucleotide hydrolysis to move DNA throughout the cell (Baxter & Funnell, 2014). Partitioning systems have also been described in temperate phages such as P1 and N15 of *Escherichia coli*, which replicate as extrachromosomal circular and linear prophages, respectively (Sternberg & Austin, 1981, Lobocka *et al.*, 2004, Ravin & Lane, 1999, Ravin, 2011, Ravin *et al.*, 2000). Although extrachromosomally-replicating prophages seem to be a relatively uncommon life style among temperate phages compared to chromosomal integration, related systems have been described in phages of diverse bacterial hosts, including *Leptospira interrogans* [lpc3, (Zhu *et al.*, 2015)], *Streptomyces sp.* [pZL12, (Zhong *et al.*, 2010)], *Vibrio vulnificus* [pVv01, (Hammerl *et al.*, 2014)] *Yersinia enterocolitica* [PY54, (Hertwig *et al.*, 2003)], *Vibrio parahaemolyticus* [VP58.5, (Zabala *et al.*, 2009)], and *Halomonas aquamarina* [ΦHAP-1, (Mobberley *et al.*, 2008)].

Although the vast majority of phages infecting actinobacterial hosts (i.e. actinobacteriophages) that group in Cluster A encode an integration cassette, a subset do not, and instead have a putative partitioning cassette located at a similar genomic position to the integration functions of closely related phages (Hatfull, 2014, Stella *et al.*, 2013). These phages must presumably encode an origin of prophage replication, although no RepA-like proteins or other such replication functions have been identified. Here we characterize the partitioning systems of mycobacteriophage RedRock and related phages. We show that RedRock forms lysogens carrying extrachromosomal prophages replicating at an average copy number of 2.4 copies/chromosome, and that a Type Ib partitioning system encoding ParA and ParB promotes prophage stability. The *parAB* genes of four different phages are expressed in lysogens and expression is autoregulated by ParB binding to a *parS* site upstream of *parA*. A putative origin of prophage replication lies adjacent to *parAB* and is associated with a highly expressed non-coding RNA in lysogenic cells. Two *parS* sites flank the *parAB* genes and are composed of multiple copies of an 8 bp directly repeated sequence motif that is recognized by ParB. Phylogenetic analysis of Par proteins shows that they span considerable sequence variation, and may be under selective pressures directed by prophage incompatibility, which we demonstrate for several pairs of *par*-containing phages.

Results

Cluster A actinobacteriophages encode diverse partitioning cassettes

Over 1,300 completely sequenced phages of actinobacterial hosts are deposited in the phagesdb database (http://phagesdb.org), including 706 entries that are fully annotated and available from GenBank or http://phagesdb.org. We therefore focused our analyses on these 706 phages, 183 of which are grouped in Cluster A, and which can be further divided into 17 subclusters (A1-A17) based on their overall genomic similarities. Most of these infect *Mycobacterium smegmatis* although one (the sole member of Subcluster A13) infects *Mycobacterium phlei* and three (all within Subcluster A15) infect *Gordonia terrae* (http://phagesdb.org). Nine of the subclusters (A2, A6, A9, A11, A13, A14, A15, A16, and A17) contain phages encoding putative homologues of previously described *parA* and *parB* genes;

in each instance *parA* and *parB* are closely linked and are genomically located where the integration cassette – containing an integrase gene and *attP* attachment site – is typically located (Fig. 1A). For example, the temperate mycobacteriophages L5 and RedRock (both in Subcluster A2) share substantial nucleotide sequence similarity and similar overall genomic organization. However, whereas the integration cassette is located between the rightwards-transcribed virion structural and assembly genes and the leftwards-transcribed right arm genes of L5 (Hatfull & Sarkis, 1993), in RedRock this position is occupied by the *parA* and *parB* genes (Fig. 1A), as it is also in the previously described phages 20ES, 40AC, and First (Stella *et al.*, 2013). The shared synteny is consistent with the integration and partitioning cassettes conferring the same biological function of prophage stability, although unlike the integrating phages, *par*-containing prophages presumably replicate autonomously and extrachromosomally.

In RedRock, genes *37* and *38* encode the *parA* and *parB* functions respectively, and are organized into an apparent operon (Fig. 1B). The genes are flanked to their immediate left and right by ~70 bp sites that include multiple copies of an 8 bp repeated motif (5'-TCGAGTnn). This organization is reminiscent of the centromere-like *parS* sites of some Type Ib plasmid partitioning systems – e.g. pSM19035 (Dmowski *et al.*, 2006) and TP228 (Zampini *et al.*, 2009) – and we designate these as *parS-L* and *parS-R* for the left and right sites respectively (Fig. 1B). We note that there are other circular permutations of the 8 bp repeat including those on the opposite strand (because of its partial palindromic nature), but six of the positions are highly conserved (present in at least 13 of the 16 repeat units at positions 1–6, in 5'-TCGAGTnn) and two (positions 7 and 8) are more varied (Fig. 1B). Similar characteristics of *parS* loci have been described in pSM19035 and TP228. Presumably one protomer of RedRock ParB recognizes each of the 8 bp motifs.

We identified 42 genomes among the sequenced actinobacteriophages containing partitioning cassettes; these include 37 *M. smegmatis* phages, 1 *M. phlei* phage, 3 *G. terrae* phages, and a previously described extrachromosomally replicating phage of *Streptomyces*, pZL12 (Fig. 2; details of phages used in the analysis are shown in Table S1) (Stella *et al.*, 2013, Zhong *et al.*, 2010). We examined the predicted ParA and ParB proteins of each of these for helix-turn-helix DNA-binding motifs (Dodd & Egan, 1990), conserved domains, and structural motifs using HHpred (Soding, 2005), and compared them to 41 previously identified partitioning systems representing the three major types (Fig. 2, S2). Several lines of evidence suggest that all of the Cluster A cassettes belong to Type Ib (Fig. 2). First, the predicted ParA proteins contain a particular variant of the Walker A ATPase motif common to Type I ParA proteins, but do not contain a predicted DNA binding motif common to Type Ia. Second, a structural motif analysis of the ParB proteins predicts C-terminal ribbon-helix-helix (RHH) motifs. The strongest hits are to pSM19035 omega (Murayama *et al.*, 2001) and TP228 ParG (Golovanov *et al.*, 2003), structurally defined members of Type Ib systems, at probabilities greater than 98% (except for Echild and 40AC). These motifs are found in Type Ib but not Type Ia systems, and are located at the C-terminal ends of the proteins (Baxter & Funnell, 2014). More broadly, the structural motif analysis shows closest similarity of the ParA and ParB proteins to domains that are specific to Type Ib ParA and ParB proteins and lack domains specific to Type Ia, II, or III proteins (see Materials and Methods). Lastly, the ParA and ParB proteins range in size from 159–228 amino acids and 84–104 amino acids,

respectively, both of which are within the common size ranges for Type Ib proteins, but smaller than common Type Ia proteins.

In most of the actinobacteriophage systems we identified, putative *parS* sites are located to the left and right of *parAB*, as in RedRock (Figs. 1B, S2A), although some lack either *parS-L* or *parS-R*. Motif searches identified putative repeated sequences related to the 8 bp identified in the RedRock *parS* sites (Fig. S2B).

The number and diversity of the partitioning systems identified here provides an opportunity to examine their evolutionary patterns. We compared the ratios of non-synonymous substitutions (K_A) to synonymous substitutions (K_S) for *parA* and *parB* between the *par*-containing actinobacteriophages (Fig. 2C) and observed that although the K_A/K_S ratios of *parA* genes are rarely above 0.3 – suggesting they are under strong purifying selection – the K_A/K_S ratios of *parB* are highly varied, and in some cases approach 1.0; furthermore, there is no apparent correlation of the *parA* and *parB* K_A/K_S ratios. The *parB* ratios are outside of the range typically regarded as indications of strong diversifying selection ($K_A/K_S > 1.0$), although diversifying selection may act only on parts of the sequences, thus moderating the overall signal. Nevertheless, there appears to be different evolutionary pressures exerted on ParA and ParB. This is consistent with the hypothesis that the CBP proteins of these Type Ib partitioning systems evolve rapidly to develop new *parS* specificities, presumably because phages with similar partitioning cassettes will exhibit incompatibility and prophage loss (Ebersbach & Gerdes, 2005, Hyland *et al.*, 2014, Radnedge *et al.*, 1996, Sergueev *et al.*, 2005). Prior analyses suggested that ParA and ParB phylogenies tend to mirror each other (Petersen *et al.*, 2009, Stella *et al.*, 2013), but quantitatively comparing their evolutionary rates is complicated because ParB homologs tend to be much more diverse and difficult to predict than their ParA counterparts (Gerdes *et al.*, 2000, Fothergill *et al.*, 2005).

The RedRock prophage replicates extrachromosomally

All of the actinobacteriophages with partitioning cassettes are predicted to be temperate, and encode repressors related to those of other Cluster A phages such as L5 and Bxb1 (Donnelly-Wu *et al.*, 1993, Jain & Hatfull, 2000); the exceptions are phages Jeffabunny, Jewelbug, and Phlei in which the repressor gene appears to have been deleted. We successfully generated stable lysogens for ten *par*-containing phages (Alma, ArcherNM, DaVinci, EagleEye, Et2Brutus, Gladiator, LadyBird, Mulciber, Pioneer, and RedRock) representing nearly all major clades of the ParB phylogeny (Fig. 2B), and showed that all of them are temperate, and not only form turbid plaques on *M. smegmatis*, but also form stable lysogens (data not shown); plaque turbidity varies considerably (the least turbid being Alma and Pioneer, the most turbid being EagleEye) likely reflecting variations in lysogeny frequency. Phage Echild forms turbid plaques but we were unable to propagate a stable lysogen. RedRock and Echild also infect and form turbid plaques on *M. tuberculosis*, Alma, Ladybird, and Pioneer infect *M. tuberculosis* at a reduced efficiency of plating (ranging from 10^{-4}-10^{-6}), and EagleEye, Gladiator, and Mulciber do not infect *M. tuberculosis*.

To address specifically whether a RedRock prophage in a lysogenic strain replicates extrachromosomally we isolated total DNA from a lysogen and performed whole genome sequencing. We reasoned that the sequencing reads mapping to the RedRock genome should

have characteristics that are distinct from those of an L5 lysogen, in which the prophage is chromosomally integrated (Hatfull & Sarkis, 1993). First, if lytic growth is tightly down-regulated then both samples should contain few if any reads corresponding to the precise ends of the viral genomes, which are otherwise readily recognized in sequence reads of viral DNA alone (Table 1). As expected, for both L5 and RedRock few reads mapped to the precise viral genome ends (Table 1). In addition, fewer than 2% of reads across the attachment sites map to a L5 viral *attP* site, with the rest mapping to the integrated *attL* and *attR* sites, consistent with the sample containing only minor amounts of viral DNA (Table 1). Second, the L5 prophage has average sequence coverage that is the same as that for the rest of the *M. smegmatis* genome, consistent with it being chromosomally integrated (Table 1), whereas in the RedRock lysogen the prophage coverage is 2.4 fold higher than the bacterial chromosome (Fig. S1). We conclude that the RedRock prophage replicates as an extrachromosomal circle with an average copy number of 2.4 per host chromosome, and note that other extrachromosomally-replicating prophages such as P1 also replicate at low copy number [P1 has a copy number of 1.6/chromosome in standard growth conditions, (Lobocka *et al.*, 2004, Prentki *et al.*, 1977)].

The RedRock genome must presumably contain two origins of DNA replication, one for lytic growth and one for extrachromosomal prophage replication, whereas L5 and other integrating phages require only a lytic replication origin. Comparison of the L5 and RedRock genomes (Fig. 1A) shows close relationships in both the left-arm and right-arm sets of genes, such that the likely location of a prophage origin is nearby the *parAB* cassette. There are no additional reading frames in this region (or elsewhere in the genome) encoding putative plasmid replication-like functions [similar to the RepA protein of P1, (Chattoraj, 2000)], and the only gene for consideration of this role is gene *36*, which is downstream of a transcriptional terminator at the end of gene *35* (Fig. 1B). However, the 62-residue gp36 protein has no database matches and has no known function; it is conserved in phages such as Rebeuca, Larenn, and Serenity, that encode integration rather than partitioning systems, and is thus unlikely to be associated with partitioning or replication functions. It is plausible that the replication origin is located in the non-coding gap between genes *36* and *37* (*parA*) and that only RNA products are required for initiation and regulation of replication. We also note that RedRock lacks additional functions associated with P1 prophage plasmid maintenance, such as a site-specific recombination system to resolve plasmid dimers [as in loxP/Cre of P1, (Austin *et al.*, 1981)], or a toxin-antitoxin addiction module [as in P1 doc/phd (Lehnherr *et al.*, 1993)]. Finally, the G-C and A-T skew patterns of RedRock and L5 are very similar, suggesting the prophage replication origin does not contribute substantially to overall biases in nucleotide composition (Fig. S3). This is consistent with the hypothesis that the integration and *ori*/partitioning cassettes are actively exchanging among this group of genomes.

RedRock parAB confers plasmid stability

To show that the RedRock *parABS* cassette is required for prophage stability we attempted to construct mutant phage derivatives in which *parA*, *parB*, or both *parA* and *parB* are deleted using BRED mutagenesis (Marinelli *et al.*, 2008). For all mutant constructions we were able to identify the presence of mutant alleles in screening of primary plaques, but

were unable to purify the mutants to homogeneity. The *parA* and *parB* constructions were repeated using a complementation system, but we again failed to purify the mutants to homogeneity (Fig. S4). Complementation of mycobacteriophage mutants has previously been found to be somewhat fickle (Dedrick *et al.*, 2013), but the general profile of mutagenesis is consistent with the *parABS* cassette being required for RedRock lytic growth; it could also be accounted for toxicity associated with loss of function.

Although we were unable to construct mutant phage derivatives, we determined whether the RedRock *parABS* system is able to confer stability to mycobacterial plasmids carrying an origin of replication (*oriM*) derived from plasmid pAL5000 (Rauzier *et al.*, 1988). These plasmids replicate at moderate copy numbers in *M. smegmatis* of about 22 copies/cell (Huff *et al.*, 2010) but are somewhat unstable, with about 35% plasmid loss following 30 generations of unselected growth (Lee *et al.*, 1991). We used an *oriM* plasmid (pLO87) containing an *mCherry* gene driven by the strong *hsp60* promoter (Oldfield & Hatfull, 2014), which confers a visible red color to *M. smegmatis* colonies and liquid cultures. This plasmid confers a notable growth disadvantage to *M. smegmatis* and in the absence of selection is lost quickly, and less than 1% of colonies retain the plasmid after 52 generations of unselected growth (Table 2); the liquid culture also lost all visible fluorescence (data not shown). In contrast, plasmid pMO01 – a derivative of pLO87 carrying the *parABS* cassette (RedRock coordinates 27,720 – 28,898) – maintained fluorescence in unselected liquid growth, and plasmid loss was constrained to about 20% after 52 generations of unselected growth (Table 2). In similar experiments in which the plasmids lack the *hsp60-mCherry* cassette and are better tolerated (e.g. pMO20), we observed only 13% loss after 52 generations of unselected growth in the absence of *parABS*, and full stabilization with inclusion of *parABS* (pMO21; Table 2).

Interruption of the *parA* gene in plasmid pMO01 destroys the plasmid stabilization effect confirming that ParA is required for stability (Table 2). We were unable to test the requirement for *parB* in this assay, as a plasmid derivative in which *parB* was interrupted fails to transform *M. smegmatis*. Removal of *parS-L* confers the same phenotype, and we hypothesize that ParB plays a regulatory role in binding to *parS-L*, and interruption of this regulation confers the non-transformable phenotype, perhaps due to toxicity of unregulated *parA* overexpression from an upstream promoter. Deletion of *parS-R* shows that it is not required for stabilization, exhibiting no significant change in plasmid retention from pMO01 (Table 2).

Expression and regulation of RedRock parAB

Because RedRock *parABS* is required for prophage stability we predict that the *parAB* genes are expressed during lysogenic growth. RNAseq analysis of a RedRock lysogen shows that the *parAB* genes are indeed expressed, although at a level approximately 5-fold lower than the phage repressor, gene *74* (Fig. 3A); the phage lytic genes are tightly down-regulated as expected. A precise transcription start site cannot be readily identified – perhaps due to RNA processing or degradation – although transcription likely begins in the *36-37* intergenic region. We also note that there is low level of expression of gene *36* (Fig. 3B).

Interestingly, there is a region of strong leftwards transcription just to the left of the *parAB* genes (Fig. 3A, B). The peak of strongest signal is approximately 200 bp long and corresponds to about 70% of the level of repressor RNA, although weaker signals extend leftwards for about another 900 bp. There are no predicted leftwards open reading frames in this region and we propose that the RNA product is either a functional or a regulatory component of the prophage origin of replication. RNAseq analysis of the lysogens of three other *par*-containing phages, Alma, EagleEye, and Pioneer, show that all make a similar leftwards-transcribed RNA adjacent to the *parAB* genes (Figs. 3C, S5), in addition to *parAB* expression. For Alma, EagleEye, and Pioneer this coincides with a predicted, rightwards-transcribed gene (*35*, *37*, and *35* respectively), but all three have very weak coding potential and are likely mis-annotations. Insertion of a 1.68 kbp fragment from RedRock (coordinates 27,232 – 28,911) that spans the *parABS* locus and intergenic transcript into a non-replicating vector did not support autonomous replication in *M. smegmatis*, so other prophage-encoded functions are likely required (data not shown).

Two other regions of RedRock prophage expression are observed. One includes genes *3*, *4* and *5*, with transcription starting within gene *2* and ending in the gene *5-6* intergenic gap. Gene *4* is predicted to encode an HNH endonuclease, gene *5* encodes a putative virion tail protein, and gene *3* is of unknown function. It is unclear whether any of the genes could be associated with prophage replication. The second region is within a non-coding region at the right end of the genome, and its role is unclear although similar expression has been observed in related but non-*parABS* phages, and is therefore also unrelated to prophage maintenance [our unpublished information; (Halleran *et al.*, 2015)]. Similar profiles are observed for the Alma, EagleEye, and Pioneer lysogens, although the expression at the genome right end is not seen in EagleEye (Fig. S5).

We also examined expression in RedRock-infected cells, both early (30 mins) and late in infection (2.5 hours). At the early time, expression is predominantly of the right arm genes, although some expression of genes at the beginning of the left arm is also observed (Fig. 3A). At the late time, expression of the right genes remains, although the left arm genes encoding the virion structure and assembly genes are expressed strongly. Interestingly, the *parAB* genes are among the most highly expressed genes early post-infection, although less so at the later time (Fig. 3A). A plausible explanation is that during liquid infection (using a multiplicity of infection of 3) a proportion of infected cells are in the process of establishing lysogeny, and that *parAB* expression is vigorous until it is subsequently down-regulated once lysogeny is established.

To further explore the regulation of *parAB* expression we constructed reporter fusion plasmids and determined promoter activity in the presence and absence of ParB (Fig. 3D). Initially a 178 bp fragment containing *parS-L* and the upstream sequences (RedRock coordinates 27,720 – 27,897) was inserted into vector pLO106 (Villanueva *et al.*, 2015) in either orientation relative to the *mCherry* reporter gene. In the forward orientation (pMO16) substantial promoter activity was observed at a level greater than that of the strong *hsp60* promoter (Oldfield & Hatfull, 2014), indicating that a highly active promoter for *parAB* expression is in this region. However, this activity is strongly down-regulated in a strain expressing RedRock ParB (Fig. 3D), consistent with transcriptional repression by binding of

ParB to *parS-L*. Interestingly, when the same DNA segment in pMO16 is inserted in the opposite orientation (pMO17), a similarly active promoter is observed, and it appears to be up-regulated by ParB (Fig. 3D). There are no clear bioinformatic signals as to the precise promoter locations, but the promoter is presumably located upstream of *parS-L* (Fig. 3B). We designate these promoters as P_{par} and P_{ori} respectively (See Fig. 1B).

Binding of RedRock ParB to parS DNA

To investigate RedRock ParB binding to the repeated sequences designated as *parS-L* and *parS-R*, we overexpressed the ParB protein and purified it to near homogeneity. Using a DNA substrate spanning the entire 666 bp *36-37* intergenic region (coordinates 27,232 – 27,897), ParB binds and forms complexes separable by native gel electrophoresis (Fig. 4A). ParB binding affinity varies somewhat between experiments (Kd = 100 nM – 300 nM), and forms discernible complexes at lower protein concentrations, but at high protein concentrations forms indistinct complexes with much slower mobilities. A similar pattern is seen using a 194 bp fragment that includes *parS-R* although the complexes are less distinct (Fig. 4A). A simple explanation is that RedRock ParB binds specifically to *parS* sequences, but due to the complexity of the locus – similar to what has been observed with the Type Ib partitioning cassettes of pSM19035 (Dmowski *et al.*, 2006) and TP228 (Zampini *et al.*, 2009, Carmelo *et al.*, 2005) – ParB may recognize individual sites with different affinities and with cooperativity at higher concentrations, forming a variety of complexes.

RedRock ParB binds to a 75 bp substrate containing the eight 8bp repeat motifs of *parS-L* to form a single complex (Fig. 4B). ParB binds substrates containing the four leftmost or four rightmost repeats similarly, such that these are equivalent for recognition. ParB also binds to a 75 bp substrate containing just the four leftmost repeats and nonspecific DNA, and forms a complex with similar mobility to the 75 bp 8-motif DNA (Fig. 4B).

ParB binds poorly, if at all, to a DNA substrate containing only a single repeat unit 5'-TCGAGTAG, and binding is enhanced when two or more repeats are present (Fig. 4C). We note, however, that there are alternative circularly permuted versions of the 8 bp repeat motif, and that 5'-TCGAGTAG is only one particular configuration. It is likely that ParB binds primarily as a dimer based on RHH structures, and as reported for other Type Ib systems (Huang *et al.*, 2011, Schreiter & Drennan, 2007); it could also recognize sites in inverted repeat orientation as described for ParG of TP228 (Zampini *et al.*, 2009). To investigate ParB-*parS* interactions, we constructed several substrates based on the parent substrate with two repeat units (Fig. 5), each with single base substitutions. Substitutions at the G in the −1 position and at the T in the +17 position in Figure 5 both show little or no impact on ParB binding, suggesting that these are either not important for recognition, or are not elements of intact binding sites in the substrates. In contrast, the T's at positions 1 and 9 both show reduced binding, such that this T position likely corresponds to the first and not the last position in the 8 bp repeat unit. Interestingly, substitutions at positions 2 – 5 and 10 – 13 have notably different impacts depending on whether they are in the first or the second 8 bp unit of the substrate. A plausible explanation is that ParB binds more weakly to the second than it does to the first of the repeats, such that binding is nearly undetectable in the 2 – 5 mutants, but is only modestly impacted by mutations at positions 10 – 13. We also note

that ParB binding to the parent substrate as well as to the mutations at positions 8, 15, 16, and 17 forms complexes with discrete mobilities, whereas many of the other mutant substrates form complexes with indiscrete mobilities. In addition, although the T at position 6 is well conserved, substituting with an A at either position 9 or 14 has little impact on binding (Fig. 5). While it is not clear what causes these patterns, it has been shown that TP228's ParG can bind to nonspecific sequence adjacent to a half-site (Carmelo *et al.*, 2005) and RedRock's ParB may be exhibiting a similar phenomenon, resulting in nucleoprotein complexes that are unstable during electrophoresis. Nonetheless, these observations are consistent with the repeated unit that is recognized by a ParB protomer being defined as 5'-TCGAGnnn.

Specificities of ParB-parS binding

The 42 partitioning systems identified in actinobacteriophages span considerable sequence diversity (Fig. 2). In general, the ParA and ParB proteins of each system appear to be co-evolving, consistent with a model in which the two proteins interact directly, as described for other partitioning systems (Baxter & Funnell, 2014). We predict that the *parS* sites similarly co-evolve and the entire systems are likely to be under selection for diversity to avoid incompatibility, as described for plasmid systems (Baxter & Funnell, 2014). We note for example that mycobacteriophages Pioneer and Alma are generally closely related (both are grouped in Subcluster A9; Fig. S6) but the partitioning cassettes are more highly diverged than the rest of the genomes, and the ParA and ParB proteins share only 60% and 44% identity, respectively.

To further explore the specificity of ParB-*parS* interactions, we examined the binding of RedRock ParB to the *parS* sites of a variety of other phages. First we asked whether RedRock ParB binds to Gladiator *parS* sites, because although the ParB proteins share only 51% identity, the consensus repeat motifs are similar (Figs. 1, S7). RedRock ParB binds to both *parS-L* and *parS-R* with only modest reduction in affinity relative to its own sites, and forms slow moving indistinct complexes as seen for RedRock *parS* (Figs. 4, 6A). We also tested RedRock ParB binding to the *parS* sites of mycobacteriophages Alma and Echild, as well as Gordonia phage KatherineG. The ParB proteins of these phages are more distant relatives of RedRock ParB (45%, 17%, and 37% amino acid sequence identity; Fig. 2) and the *parS* sites have related but different 8 bp repeat consensus sequences (Fig. S7). We observed little or no RedRock ParB binding to any of these sites (Fig. 6A).

We also overexpressed and purified the ParB protein of phage Alma. Alma ParB binds to both Alma *parS-L* and *parS-R* sites and forms slowly migrating complexes. Somewhat surprisingly, Alma ParB is more promiscuous than RedRock ParB and is able to bind to both RedRock *parS-L* and *parS-R* sites (Figs. 6B, S7). Alma ParB also binds albeit with somewhat lower affinity to Gladiator *parS* sites (Fig. 6B, Fig. S7), and also to Echild *parS-L* despite the divergence of the motif consensus sequences, but not to KatherineG parS-R (Fig. S7). Similar to the analysis of RedRock *parS* individual repeat positions, these observations show that specificity of the partitioning systems is complex, and that although there is substantial sequence variation, ParB proteins can range broadly in their specificities.

Partitioning-mediated prophage incompatibility

To test whether *par*-containing prophages exhibit incompatibility, we identified pairs of mycobacteriophages containing *par* cassettes in which the immunity repressors and their operator/stoperator binding sites are sufficiently different that they are heteroimmune. As a control, we used phages Bxb1 and RedRock, which are heteroimmune, but unlike RedRock, Bxb1 has a canonical integration cassette (Kim *et al.*, 2003). Starting with a RedRock lysogen, we attempted to construct double lysogens by superinfection with Bxb1, Alma, or Pioneer, followed by propagation through several rounds of purification and growth in liquid culture, and testing for superinfection immunity to each of the phages throughout the experiment (see Materials and Methods and Fig. S8 for details). For the RedRock/Bxb1 infections, we successfully generated double lysogens, confirming they are fully compatible. In contrast, for the RedRock/Alma and RedRock/Pioneer pairs, we identified double lysogens after the initial superinfection, but were unable to propagate the strains through purification. Nearly all colonies tested resulted in a single lysogen of either Alma or Pioneer in which the RedRock prophage had been displaced. These pairs of *par*-containing phages thus clearly exhibit incompatibility. This is consistent with the non-reciprocal *parS* recognition of the Alma and RedRock ParB proteins (Fig. 6), and we predict that Pioneer ParB may behave similarly, although we cannot discount that incompatibility results from the prophage replication systems, rather than partitioning *per se*. In similar experiments where either RedRock or Alma superinfected a Gladiator lysogen, Alma failed to displace Gladiator, RedRock displaced Gladiator 40% of the time to generate single RedRock lysogens, and no double lysogens were obtained. Alma and L5 (an integrating phage) co-infections of wild type *M. smegmatis* successfully generated double lysogens, as seen with RedRock and Bxb1.

To determine whether the *par* systems specifically contribute to incompatibility, we tested the compatibility of plasmid pMO01 – which contains the *parABS* cassette but not the putative RNA-encoding replication functions to its left (see above) – with a RedRock lysogen. Plasmid pMO01 was introduced into RedRock lysogenic cells by electroporation, and kanamycin resistant transformants were selected (Fig. 7A). Three independent transformants were propagated and tested for lysogeny by a standard spontaneous phage release assay. All transformants were shown to have lost the RedRock prophage (Fig. 7B). In contrast, control transformants carrying pLO87 DNA (which lacks *parABS*) all maintained RedRock lysogeny, and lysogeny was maintained in L5 lysogens that carry an integrated prophage. Plasmid pMO01 thus displays incompatibility specifically with the RedRock prophage. Phage release was also observed by pMO01 transformants of the EagleEye lysogen suggesting partial incompatibility between the RedRock and EagleEye *par* systems. However, we note that this may be exacerbated by the relatively high plasmid copy number [~20 copies/chromosome (Huff *et al.*, 2010)] relative to the EagleEye prophage, which we assume has a similarly copy number of ~2.4 copies/chromosome as RedRock.

Discussion

Phage-encoded partitioning systems are not uncommon among temperate phages of the actinobacteria although all are found within a group of related phages defined as Cluster A

[the exception is pZL12 which was identified as a plasmid in Streptomyces and is unrelated to the other phages (Zhong *et al.*, 2010)]. Approximately 20% of the Cluster A phages have partitioning cassettes and the remainder have integration cassettes, distributed between tyrosine- and serine-integrase systems. These *par* systems considerably expand the number of previously described phage-encoded partitioning systems. All of the Cluster A phage *par* components belong to the Type Ib system, which have not been previously identified in phage genomes.

Phage RedRock forms stable lysogens in which the prophage replicates extrachromosomally at an average copy number of 2.4 copies/chromosome, with the *parABS* system promoting prophage maintenance. RedRock ParB binds to two *parS* sites flanking the *parAB* genes and plays a regulatory role in addition to its presumed role in prophage segregation. Upon infection, RNAseq analysis shows strong unregulated expression of *parAB* from a promoter located between gene *36* and *parA*, which is then down regulated in lysogeny through the binding of ParB to *parS-L*. ParB could also play a role in terminating transcription of *parAB* by its binding to *parS-R*. The inability to construct a deletion derivative of *parB* can be explained by the toxic consequences of *parA* overexpression, although the inability to construct a lytically-proficient deletion of *parA* is more puzzling. It is possible that *parB* expression is inhibitory to lytic growth unless *parA* is also expressed.

In general, the actinobacteriophage *parS* sites are composed of 5–10 copies of tandemly repeated 8 bp motifs. We propose that one ParB protomer binds to each of these motifs, but that occupancy may be stimulated by several factors, similar to other Type Ib systems, such as those described in pSM19035 (Dmowski *et al.*, 2006; Schreiter & Drennan, 2007), TP228 (Carmelo *et al.*, 2005; Zampini *et al.*, 2009), and pCXC100 (Huang *et al.*, 2011). For instance, repeats that vary in sequence can be bound with varying affinities, the repeats can occur in multiple orientations that can impact affinity, and binding of tandem sites can be cooperative. The N-terminal tail of the CBP, which tends to be unstructured, has been shown to enhance binding stability through transient interactions with the folded C-terminal region. Taken together, while the current study investigates the general binding behaviors of several actinobacteriophage partitioning systems, further investigations are needed to elucidate the binding interactions in greater detail. Additionally, we note that the phage-encoded *parS* sites are distinctly different from the palindromic sites that form the host *parS* site in *Mycobacterium tuberculosis* and *M. smegmatis* (5’-GTTTCACGTGAAAC 3’) or *parS* in *Bacillus subtilis* (5’-TGTTCCACGTGAAACT 3’) (Lin & Grossman, 1998, Jakimowicz *et al.*, 2007).

The partitioning cassettes span considerable diversity, and we note that the partitioning cassettes of phages Echild and 40AC are noticeably different than other Cluster A phages (Fig. 2). Their *parA* genes can be readily identified (Fig. 2A), but their *parB* genes are more divergent (Fig. 2B). Structural domain analysis shows that Echild’s ParB has noticeably fewer Type Ib domain hits than other Cluster A phages, and 40AC’s ParB has no predicted domains of any partitioning type. Additionally, the tandem repeat program, etandem (Rice *et al.*, 2000), predicts *parS-L* sites for Echild and 40AC, but no *parS-R* for 40AC, and an Echild *parS-R* that is distinct from its *parS-L* and thus may not represent a ParB recognition sequence (Fig. S2). A prior study failed to isolate 40AC stable lysogens (Stella *et al.*, 2013),

suggesting the predicted ParB may not be functional. We have successfully isolated an Echild lysogen that exhibits superinfection immunity (data not shown), although lysogeny is not stably maintained and non-lysogenic derivatives accumulate at high frequency (data not shown). The K_A/K_S ratios indicate that *parA* and *parB* are under selection, and is thus plausible that Echild and 40AC have a *bona fide* partitioning cassette, but that does not function efficiently in *M. smegmatis*.

The *par* actinobacteriophages are broadly distributed within Cluster A, and are found in over half of the component subclusters. The ParA and ParB sequences themselves span considerable sequence diversity, illustrated by the most distantly related ParB proteins (e.g. Echild and RedRock) sharing only 17% amino sequence identity. Because lysogeny could not be established by two different extrachromosomal phages in the same cell, it is likely that there is selective pressure to diversify the partitioning systems in order to avoid incompatibility, as seen in plasmid systems (Radnedge *et al.*, 1996, Sergueev *et al.*, 2005, Hyland *et al.*, 2014). This could occur at two levels: by diversification of the ParB and the *parS* sites that they recognize, or through variation in the interactions between the interacting components of ParA and ParB. It seems likely that both play important roles, and we show here that the ParB proteins can distinguish between *parS* sites of distantly related phages. The pairs of phages that could be readily tested for compatibility (RedRock and Alma, RedRock and Pioneer) do show marked incompatibility, and we demonstrated *par*-mediated incompatibility using a RedRock *par*-containing recombinant plasmid and a RedRock prophage.

The *par*-containing actinobacteriophages replicate extrachromosomally as low copy number prophages, and thus must have an origin of replication that is absent from the integrating phages. The most obvious location for the origin is adjacent to the *parABS* cassette with which it can co-evolve, and this is consistent with genome comparisons of pairs of closely-related phages encoding integration and partitioning cassettes. However, none of the extrachromosomal phages encode RepA or other plasmid-like replication proteins, but RedRock as well as three other lysogens express an RNA implicated in prophage replication. The nucleotide sequences of the ~300 bp regions to the left of *parAB*S are highly varied, and although folded RNA structures can be predicted, there is little in common to these phages that reveals the functional components. Efforts to clone RedRock DNA fragments that promote autonomous replication have thus far been unsuccessful.

The actinobacteriophage partitioning cassettes have three potential utilities for bacterial genetics. First, the pAL5000-derived plasmid vectors commonly used in mycobacterial genetics are often poorly maintained in the absence of selection, and the *parABS* cassettes of RedRock and related phages can be used to confer plasmid maintenance (Table 2). There are a variety of particular applications where this may be useful, but notably where recombinants are tested in animal model systems or as live vaccine candidates, and where expression levels derived from the use of multicopy plasmids is desirable. Second, although the origin of replication has yet to be precisely determined, the *ori-par* functions have the potential to provide a new series of low copy number plasmid vectors that are fully compatible with extant vector systems. Lastly, the ability of ParB to bind to *parS* in multiple copies offers the possibility that ParB-GFP fusion proteins could be used to geographically

identify chromosomal segments in the cell by introduction of *parS* sites into the host genome. This approach has worked well in *E. coli* using P1 ParB (Erdmann *et al.*, 1999), and the variety of actinobacteriophage partitioning cassettes provide multiple systems that could be used in combination and are anticipated to be well-expressed. The phylogenetic and structural domain analyses of the partitioning systems may enhance the development of similar tools in other bacterial hosts including *Leptospira* [exploiting lcp1, lcp2, and lcp3, (Zhu *et al.*, 2015)], *Streptomyces* [plasmids pZL12, pSLE1, and pSLE2 (Gomez-Escribano *et al.*, 2015, Zhong *et al.*, 2010)], and in *Vibrio* [using ΦHAP-1, pVv01, and Vp58.5 (Mobberley *et al.*, 2008, Hammerl *et al.*, 2014, Zabala *et al.*, 2009)].

Materials and Methods

Bacteria and plasmids

Liquid cultures of *M. smegmatis* mc^{2}155 and the lysogenic derivatives were grown in Middlebrook 7H9 at 37°C with shaking. Phage infection assays on solid media were performed using exponentially growing cultures plated with a soft top agar layer on Middlebrook 7H10 plates. Plasmids used in this study are listed in Table S2. Plasmid pMO01 is a derivative of pLO87 (Oldfield & Hatfull, 2014) an extrachromosomal shuttle vector with P_{hsp60} driving *mCherry* expression, with the RedRock *par* cassette (coordinates 27,720 – 28,898) cloned downstream of *mCherry*. Several derivatives of pMO01 were constructed, including pMO02 and pMO03, which contain translational termination codons early in the *parA* and *parB* open reading frames, respectively. Plasmids pMO04 and pMO05 are derivatives of pMO01 with deletions of *parS-L* and *parS-R*, respectively. Plasmid pMO20 and pMO21 are derivatives of pLO87 and pMO01, respectively, in which the *hsp60-mCherry* cassette has been removed. Plasmid pMO16 and pMO17 are derivatives of the extrachromosomal shuttle vector pLO106 (Villanueva *et al.*, 2015), which contains phage BPs p6 driving *mCherry* expression. A 178 bp fragment of RedRock (coordinates 27,720 – 27,897) was cloned in the forward orientation (pMO16) and reverse orientation (pMO17) downstream of p6. Plasmid pMO15 is a derivative of the integration-proficient vector pJV39 carrying P_{hsp60} fused to RedRock *parB*. Plasmids pJC04 and pJC05 are derivatives of vector pLAM12 (Marinelli *et al.*, 2008) containing RedRock *parA* and *parB*, respectively.

Plasmid Maintenance Assays

M. smegmatis transformants carrying various plasmids were grown in liquid culture with antibiotic selection for plasmid maintenance for approximately 24 hours or until saturated. Cultures were then diluted 1:10,000 into antibiotic-free media and re-grown to saturation (approximately 13 generations), and subsequent rounds of dilution were used to increase the number of rounds of unselected growth. Cultures were then plated onto solid media, and colonies were scored for plasmid maintenance (red) or for plasmid loss (white). Statistical significance of changes in plasmid retention was computed using two-sample two-tailed t-test of the retention level from three independent replicates.

Promoter Strength Assays

Individual colonies of *M. smegmatis* transformants carrying various plasmids were grown in liquid media with shaking, at 37°C, for 24–48 hrs. Readings of *mCherry* fluorescence were

taken as described previously (Oldfield & Hatfull, 2014), except that the measurement of optical density was taken at 600 nm in a Beckman Coulter DU530. Fluorescence units are reported as the amount of fluorescence per area per OD_{600}.

DNA sequencing and RNAseq

DNA from a 2 ml sample of the RedRock or L5 lysogen was extracted from late logarithmically growing cells (OD_{600} approximately 1.0) using the Wizard kit (Promega) according to the manufacturers' instructions. DNA was quantified using Qubit and libraries were prepped using the TruSeq Library Kit (Illumina) according to the manufacturers' instructions. The completed libraries were run on an Illumina MiSeq and data was evaluated using CLC Genomics software. For RNAseq, total RNA was isolated from *M. smegmatis* cultures in exponential growth, as well as 30 min and 2.5 hrs after infection with RedRock at a multiplicity of infection of three. DNA was removed using the DNA-free kit (Ambion) and rRNA was depleted using the Ribo-Zero kit (Illumina). Libraries were prepared using a TruSeq Stranded RNAseq kit (Illumina) and run on an Illumina MiSeq: one lane for each RedRock sample, and one multiplexed lane for wild type *M. smegmatis*, Alma, Pioneer, and EagleEye lysogens. The fastq reads were analyzed for overall quality using FastQC (Andrews, S. http://www.bioinformatics.babraham.ac.uk/projects/fastqc/), trimmed at the 5' and 3' ends with cutadapt (Martin, 2011) using a quality score threshold of 30, and then mapped simultaneously to the *M. smegmatis* and RedRock genomes with Bowtie2 (Langmead & Salzberg, 2012). SAMtools (Li *et al.*, 2009) and BEDtools (Quinlan & Hall, 2010) were used to process reads that aligned to exactly one locus (as computed by Bowtie2) and calculate strand-specific genome coverage. Integrative Genomics Viewer (Thorvaldsdottir *et al.*, 2013) was used to visualize the data. The RNAseq data set is deposited in the Gene Expression Omnibus (GEO) with accession number GSE79010.

Purification of ParB

The *parB* gene was PCR amplified from RedRock or Alma and inserted into plasmid pET28a (Novagen) such as to include a His_6 tag at the C-termini of each protein. After verification by sequencing, the resulting plasmids (pJC02 and pWN01, respectively) were transformed into BL21* (DE3)pLysS cells and grown to an OD_{600} of 0.5 at 37°C in LB. His-ParB expression was induced by the addition of 1 mM IPTG at 37°C for 3 hrs. Cells were pelleted, resuspended in 5 ml/g of lysis buffer (50 mM Tris-HCL (pH8), 300 mM NaCl and 5% glycerol), and sonicated. The sonicated cells were centrifuged and the cleared lysate was applied to a nickel column using Ni-NTA column (Qiagen). The column was washed with lysis buffer, 10 mM, and 50 mM imidazole and the proteins eluted with 150 mM imidazole. Fractions were collected and dialyzed in lysis buffer containing 30–50% glycerol overnight at 4°C.

Electrophoretic Mobility Shift Assays

DNA substrates were prepared using either gel-extracted PCR substrates or annealed synthetic oligonucleotides (IDT & Invitrogen) (Table S3). Double stranded DNA substrates were 5'-end radiolabeled using ATP, [γ-^{32}P] with T4 polynucleotide kinase (Roche) at 37°C for 30 min and cleaned up using G-50 sephadex columns. 5–10 ng of radiolabeled substrates were incubated at room temperature for 30 min with indicated concentrations of ParB in a

buffer containing 20 mM Tris pH 7.5, 10 mM EDTA, 25 mM NaCl, 10 mM spermadine, 1 mM DTT and 1 μg calf thymus DNA in a total volume of 10 μl. The DNA-protein samples were then resolved on a 5% native polyacrylamide gel run at 4°C. The gel was dried and exposed to a phosphorimaging plate, then scanned using a Fuji 5,000 Phosphorimager. Dissociation constants (Kd) were calculated as the protein concentration at which 50% of the input DNA was protein-bound.

Phylogenetic analysis of partitioning cassettes

A database (Actinobacteriophage_706) was constructed using the program Phamerator as described previously (Cresawn *et al.*, 2011, Pope *et al.*, 2015). The database contains 706 genomes of phages infecting Actinobacterial hosts coding for 70,341 genes that are grouped according to their sequence similarity into 9,523 phamilies (phams). This database contains 42 genomes with predicted partitioning cassettes. The protein sequences for 41 other putative and characterized NTPase and CBP genes from partitioning cassettes were identified from the literature and retrieved from NCBI (see Table S1). This non-exhaustive list of *par* cassettes represents cassettes from each partitioning type [Ia, Ib, II, III, or unknown, depending on how cassettes have been previously categorized in (Gerdes *et al.*, 2000, Ebersbach & Gerdes, 2005, Schumacher, 2012)], from various replicon types (chromosomal, plasmid, or phage), and from various bacterial host genera. In some replicons where there was a previously predicted NTPase but no accompanying CBP, there nevertheless tended to be an ORF immediately downstream in an apparent operon with *parA*, and these sequences were used as a potential CBP in the phylogeny. Protein sequences were aligned in Seaview (Gouy *et al.*, 2010) using ClustalO and a phylogeny was created using the BioNJ algorithm with observed distances. A bootstrap analysis was performed with 100 replicates. Trees generated using other methods were comparable. Phylogenies were visualized and appended with genomic data using Evolview (Zhang *et al.*, 2012).

Prediction of partitioning types

HHpred (Soding, 2005) was used to predict the types of partitioning system for the cassettes used in this study. First, each partitioning protein was analyzed using HHpred with the pdb70_15Feb16 database and with default settings as of February 22, 2016. The top 100 domain hits per gene that exceeded a homologous relationship probability (as computed by the program) cutoff of 90% were retained. All structural domain hits returned for the group of partitioning cassettes that have been previously categorized as Type Ia, Ib, II, or III (see Table S1) were assigned a partitioning type category as follows. If the domain was found in one or more genes from only one partitioning cassette type category, the domain was assigned the same partitioning type category, reflecting that in this analysis the domain is only found in genes of that particular partitioning type. If the domain was present in genes from more than one partitioning type, it was categorized as “nonspecific.” Next, the frequency of each domain category was calculated for partitioning genes in the entire set of 83 partitioning cassettes. Finally, stacked bar graphs of these frequencies were generated for each gene to provide a qualitative measure of how similar each partitioning gene is to previously characterized partitioning genes. The analysis was done separately for *parA* and *parB* genes.

ParA and ParB coevolution analysis

The rate of evolution of the actinobacteriophage *parA* and *parB* genes were analyzed as follows. Of the 42 phages in the Actinobacteriophage_706 database, Echild, 40AC, and pZL12 were not used; their ParA and/or ParB genes did not group with the rest of the actinobacteriophages in the protein sequence phylogenies, suggesting they were too distantly related for meaningful comparison. Of the remaining 39 phages, redundant DNA sequences of each partitioning gene were removed, reducing the list to a total of 27 phages that contain unique *parA* and *parB* sequences available for analysis (see Table S1); *parA* and *parB* genes were processed separately. DNA sequences were aligned at the codon level using webPRANK (Loytynoja & Goldman, 2010) and processed using the kaks tool in the 'seqinr' R package to compute the pairwise K_A, K_S, and K_A/K_S values. The K_A/K_S ratios for all pairwise comparisons that had a $K_S < 2.0$ were retained, and a scatter plot of the matching *parA* and *parB* ratios was generated.

Supplementary Material

Refer to Web version on PubMed Central for supplementary material.

Acknowledgments

We thank Carlos Guerrero for excellent technical assistance, Valerie Villanueva and Lauren Oldfield for experimental assistance and student supervision, and Charles Bowman for DNA sequencing assistance. This was work was supported by grants from the National Institutes of Health (GM116884) and Howard Hughes Medical Institute (54308198) to GFH, and National Science Foundation pre-doctoral fellowship to TNM (1247842). No authors have conflicts of interest. Author contributions: RMD, TNM, WLN, JCCRR, MRO, RER, DJS, DAR, designed, performed and interpreted experiments; GFH designed and interpreted experiments; RMD, TNM, and GFH wrote the manuscript.

References

Austin S, Ziese M, Sternberg N. A novel role for site-specific recombination in maintenance of bacterial replicons. Cell. 1981; 25:729–736. [PubMed: 7026049]

Baxter JC, Funnell BE. Plasmid Partition Mechanisms. Microbiol Spectr. 2014:2.

Bourhy P, Frangeul L, Couve E, Glaser P, Saint Girons I, Picardeau M. Complete nucleotide sequence of the LE1 prophage from the spirochete Leptospira biflexa and characterization of its replication and partition functions. J Bacteriol. 2005; 187:3931–3940. [PubMed: 15937155]

Broussard GW, Oldfield LM, Villanueva VM, Lunt BL, Shine EE, Hatfull GF. Integration-dependent bacteriophage immunity provides insights into the evolution of genetic switches. Mol Cell. 2013; 49:237–248. [PubMed: 23246436]

Brown KL, Sarkis GJ, Wadsworth C, Hatfull GF. Transcriptional silencing by the mycobacteriophage L5 repressor. Embo J. 1997; 16:5914–5921. [PubMed: 9312049]

Carmelo E, Barilla D, Golovanov AP, Lian LY, Derome A, Hayes F. The unstructured N-terminal tail of ParG modulates assembly of a quaternary nucleoprotein complex in transcription repression. J Biol Chem. 2005; 280:28683–28691. [PubMed: 15951570]

Chattoraj DK. Control of plasmid DNA replication by iterons: no longer paradoxical. Mol Microbiol. 2000; 37:467–476. [PubMed: 10931340]

Cresawn SG, Bogel M, Day N, Jacobs-Sera D, Hendrix RW, Hatfull GF. Phamerator: a bioinformatic tool for comparative bacteriophage genomics. BMC Bioinformatics. 2011; 12:395. [PubMed: 21991981]

Dedrick RM, Marinelli LJ, Newton GL, Pogliano K, Pogliano J, Hatfull GF. Functional requirements for bacteriophage growth: gene essentiality and expression in mycobacteriophage Giles. Mol Microbiol. 2013; 88:577–589. [PubMed: 23560716]

Dmowski M, Sitkiewicz I, Ceglowski P. Characterization of a novel partition system encoded by the delta and omega genes from the streptococcal plasmid pSM19035. J Bacteriol. 2006; 188:4362–4372. [PubMed: 16740943]

Dodd IB, Egan JB. Improved detection of helix-turn-helix DNA-binding motifs in protein sequences. Nucleic Acids Res. 1990; 18:5019–5026. [PubMed: 2402433]

Donnelly-Wu MK, Jacobs WR Jr, Hatfull GF. Superinfection immunity of mycobacteriophage L5: applications for genetic transformation of mycobacteria. Mol Microbiol. 1993; 7:407–417. [PubMed: 8459767]

Ebersbach G, Gerdes K. Plasmid segregation mechanisms. Annu Rev Genet. 2005; 39:453–479. [PubMed: 16285868]

Erdmann N, Petroff T, Funnell BE. Intracellular localization of P1 ParB protein depends on ParA and parS. Proc Natl Acad Sci U S A. 1999; 96:14905–14910. [PubMed: 10611311]

Fothergill TJ, Barilla D, Hayes F. Protein diversity confers specificity in plasmid segregation. J Bacteriol. 2005; 187:2651–2661. [PubMed: 15805511]

Gerdes K, Moller-Jensen J, Bugge Jensen R. Plasmid and chromosome partitioning: surprises from phylogeny. Mol Microbiol. 2000; 37:455–466. [PubMed: 10931339]

Golovanov AP, Barilla D, Golovanova M, Hayes F, Lian LY. ParG, a protein required for active partition of bacterial plasmids, has a dimeric ribbon-helix-helix structure. Mol Microbiol. 2003; 50:1141–1153. [PubMed: 14622405]

Gomez-Escribano JP, Castro JF, Razmilic V, Chandra G, Andrews B, Asenjo JA, Bibb MJ. The Streptomyces leeuwenhoekii genome: de novo sequencing and assembly in single contigs of the chromosome, circular plasmid pSLE1 and linear plasmid pSLE2. BMC Genomics. 2015; 16:485. [PubMed: 26122045]

Gouy M, Guindon S, Gascuel O. SeaView version 4: A multiplatform graphical user interface for sequence alignment and phylogenetic tree building. Mol Biol Evol. 2010; 27:221–224. [PubMed: 19854763]

Halleran A, Clamons S, Saha M. Transcriptomic Characterization of an Infection of Mycobacterium smegmatis by the Cluster A4 Mycobacteriophage Kampy. PLoS One. 2015; 10:e0141100. [PubMed: 26513661]

Hammerl JA, Klevanskaa K, Strauch E, Hertwig S. Complete Nucleotide Sequence of pVv01, a P1-Like Plasmid Prophage of Vibrio vulnificus. Genome announcements. 2014:2.

Hatfull GF. Mycobacteriophages: genes and genomes. Annu Rev Microbiol. 2010; 64:331–356. [PubMed: 20528690]

Hatfull GF. The secret lives of mycobacteriophages. Adv Virus Res. 2012; 82:179–288. [PubMed: 22420855]

Hatfull GF. Molecular Genetics of Mycobacteriophages. Microbiology Spectrum. 2014; 2:1–36. [PubMed: 25328854]

Hatfull GF, Jacobs-Sera D, Lawrence JG, Pope WH, Russell DA, Ko CC, Weber RJ, Patel MC, Germane KL, Edgar RH, Hoyte NN, Bowman CA, Tantoco AT, Paladin EC, Myers MS, Smith AL, Grace MS, Pham TT, O'Brien MB, Vogelsberger AM, Hryckowian AJ, Wynalek JL, Donis-Keller H, Bogel MW, Peebles CL, Cresawn SG, Hendrix RW. Comparative Genomic Analysis of 60 Mycobacteriophage Genomes: Genome Clustering, Gene Acquisition, and Gene Size. J Mol Biol. 2010; 397:119–143. [PubMed: 20064525]

Hatfull GF, Sarkis GJ. DNA sequence, structure and gene expression of mycobacteriophage L5: a phage system for mycobacterial genetics. Mol Microbiol. 1993; 7:395–405. [PubMed: 8459766]

Hertwig S, Klein I, Schmidt V, Beck S, Hammerl JA, Appel B. Sequence analysis of the genome of the temperate Yersinia enterocolitica phage PY54. J Mol Biol. 2003; 331:605–622. [PubMed: 12899832]

Huang L, Yin P, Zhu X, Zhang Y, Ye K. Crystal structure and centromere binding of the plasmid segregation protein ParB from pCXC100. Nucleic Acids Res. 2011; 39:2954–2968. [PubMed: 21123191]

Huff J, Czyz A, Landick R, Niederweis M. Taking phage integration to the next level as a genetic tool for mycobacteria. Gene. 2010; 468:8–19. [PubMed: 20692326]

Hyland EM, Wallace EW, Murray AW. A model for the evolution of biological specificity: a cross-reacting DNA-binding protein causes plasmid incompatibility. J Bacteriol. 2014; 196:3002–3011. [PubMed: 24914185]

Jain S, Hatfull GF. Transcriptional regulation and immunity in mycobacteriophage Bxb1. Mol Microbiol. 2000; 38:971–985. [PubMed: 11123672]

Jakimowicz D, Brzostek A, Rumijowska-Galewicz A, Zydek P, Dolzblasz A, Smulczyk-Krawczyszyn A, Zimniak T, Wojtasz L, Zawilak-Pawlik A, Kois A, Dziadek J, Zakrzewska-Czerwinska J. Characterization of the mycobacterial chromosome segregation protein ParB and identification of its target in Mycobacterium smegmatis. Microbiology. 2007; 153:4050–4060. [PubMed: 18048919]

Kim AI, Ghosh P, Aaron MA, Bibb LA, Jain S, Hatfull GF. Mycobacteriophage Bxb1 integrates into the Mycobacterium smegmatis groEL1 gene. Mol Microbiol. 2003; 50:463–473. [PubMed: 14617171]

Langmead B, Salzberg SL. Fast gapped-read alignment with Bowtie 2. Nat Methods. 2012; 9:357–359. [PubMed: 22388286]

Lee MH, Pascopella L, Jacobs WR Jr, Hatfull GF. Site-specific integration of mycobacteriophage L5: integration-proficient vectors for Mycobacterium smegmatis, Mycobacterium tuberculosis, and bacille Calmette-Guerin. Proc Natl Acad Sci U S A. 1991; 88:3111–3115. [PubMed: 1901654]

Lehnherr H, Maguin E, Jafri S, Yarmolinsky MB. Plasmid addiction genes of bacteriophage P1: doc, which causes cell death on curing of prophage, and phd, which prevents host death when prophage is retained. J Mol Biol. 1993; 233:414–428. [PubMed: 8411153]

Li H, Handsaker B, Wysoker A, Fennell T, Ruan J, Homer N, Marth G, Abecasis G, Durbin R. S. Genome Project Data Processing. The Sequence Alignment/Map format and SAMtools. Bioinformatics. 2009; 25:2078–2079. [PubMed: 19505943]

Lin DC, Grossman AD. Identification and characterization of a bacterial chromosome partitioning site. Cell. 1998; 92:675–685. [PubMed: 9506522]

Lobocka MB, Rose DJ, Plunkett G 3rd, Rusin M, Samojedny A, Lehnherr H, Yarmolinsky MB, Blattner FR. Genome of bacteriophage P1. J Bacteriol. 2004; 186:7032–7068. [PubMed: 15489417]

Loytynoja A, Goldman N. webPRANK: a phylogeny-aware multiple sequence aligner with interactive alignment browser. BMC Bioinformatics. 2010; 11:579. [PubMed: 21110866]

Marinelli LJ, Piuri M, Swigonova Z, Balachandran A, Oldfield LM, van Kessel JC, Hatfull GF. BRED: a simple and powerful tool for constructing mutant and recombinant bacteriophage genomes. PLoS ONE. 2008; 3:e3957. [PubMed: 19088849]

Mobberley JM, Authement RN, Segall AM, Paul JH. The temperate marine phage PhiHAP-1 of Halomonas aquamarina possesses a linear plasmid-like prophage genome. J Virol. 2008; 82:6618–6630. [PubMed: 18448537]

Murayama K, Orth P, de la Hoz AB, Alonso JC, Saenger W. Crystal structure of omega transcriptional repressor encoded by Streptococcus pyogenes plasmid pSM19035 at 1.5 A resolution. J Mol Biol. 2001; 314:789–796. [PubMed: 11733997]

Oldfield LM, Hatfull GF. Mutational analysis of the mycobacteriophage BPs promoter PR reveals context-dependent sequences for mycobacterial gene expression. J Bacteriol. 2014; 196:3589–3597. [PubMed: 25092027]

Petersen J, Brinkmann H, Pradella S. Diversity and evolution of repABC type plasmids in Rhodobacterales. Environ Microbiol. 2009; 11:2627–2638. [PubMed: 19601964]

Pope WH, Bowman CA, Russell DA, Jacobs-Sera D, Asai DJ, Cresawn SG, Jacobs WR, Hendrix RW, Lawrence JG, Hatfull GF. G. Science Education Alliance Phage Hunters Advancing, S. Evolutionary, R. Phage Hunters Integrating, Education, & C. Mycobacterial Genetics. Whole genome comparison of a large collection of mycobacteriophages reveals a continuum of phage genetic diversity. Elife. 2015; 4:e06416. [PubMed: 25919952]

Pope WH, Jacobs-Sera D, Russell DA, Peebles CL, Al-Atrache Z, Alcoser TA, Alexander LM, Alfano MB, Alford ST, Amy NE, Anderson MD, Anderson AG, Ang AAS, Ares M Jr, Barber AJ, Barker LP, Barrett JM, Barshop WD, Bauerle CM, Bayles IM, Belfield KL, Best AA, Borjon A Jr, Bowman CA, Boyer CA, Bradley KW, Bradley VA, Broadway LN, Budwal K, Busby KN,

Campbell IW, Campbell AM, Carey A, Caruso SM, Chew RD, Cockburn CL, Cohen LB, Corajod JM, Cresawn SG, Davis KR, Deng L, Denver DR, Dixon BR, Ekram S, Elgin SCR, Engelsen AE, English BEV, Erb ML, Estrada C, Filliger LZ, Findley AM, Forbes L, Forsyth MH, Fox TM, Fritz MJ, Garcia R, George ZD, Georges AE, Gissendanner CR, Goff S, Goldstein R, Gordon KC, Green RD, Guerra SL, Guiney-Olsen KR, Guiza BG, Haghighat L, Hagopian GV, Harmon CJ, Harmson JS, Hartzog GA, Harvey SE, He S, He KJ, Healy KE, Higinbotham ER, Hildebrandt EN, Ho JH, Hogan GM, Hohenstein VG, Holz NA, Huang VJ, Hufford EL, Hynes PM, Jackson AS, Jansen EC, Jarvik J, Jasinto PG, Jordan TC, Kasza T, Katelyn MA, Kelsey JS, Kerrigan LA, Khaw D, Kim J, Knutter JZ, Ko C-C, Larkin GV, Laroche JR, Latif A, et al. Expanding the Diversity of Mycobacteriophages: Insights into Genome Architecture and Evolution. PLoS ONE. 2011; 6:e16329. [PubMed: 21298013]

Prentki P, Chandler M, Caro L. Replication of prophage P1 during the cell cycle of Escherichia coli. Mol Gen Genet. 1977; 152:71–76. [PubMed: 325389]

Quinlan AR, Hall IM. BEDTools: a flexible suite of utilities for comparing genomic features. Bioinformatics. 2010; 26:841–842. [PubMed: 20110278]

Radnedge L, Davis MA, Austin SJ. P1 and P7 plasmid partition: ParB protein bound to its partition site makes a separate discriminator contact with the DNA that determines species specificity. EMBO J. 1996; 15:1155–1162. [PubMed: 8605886]

Rauzier J, Moniz-Pereira J, Gicquel-Sanzey B. Complete nucleotide sequence of pAL5000, a plasmid from Mycobacterium fortuitum. Gene. 1988; 71:315–321. [PubMed: 3224826]

Ravin N, Lane D. Partition of the linear plasmid N15: interactions of N15 partition functions with the sop locus of the F plasmid. J Bacteriol. 1999; 181:6898–6906. [PubMed: 10559154]

Ravin NV. N15: the linear phage-plasmid. Plasmid. 2011; 65:102–109. [PubMed: 21185326]

Ravin V, Ravin N, Casjens S, Ford ME, Hatfull GF, Hendrix RW. Genomic sequence and analysis of the atypical temperate bacteriophage N15. J Mol Biol. 2000; 299:53–73. [PubMed: 10860722]

Reyes-Lamothe R, Nicolas E, Sherratt DJ. Chromosome replication and segregation in bacteria. Annu Rev Genet. 2012; 46:121–143. [PubMed: 22934648]

Rice P, Longden I, Bleasby A. EMBOSS: the European Molecular Biology Open Software Suite. Trends Genet. 2000; 16:276–277. [PubMed: 10827456]

Schreiter ER, Drennan CL. Ribbon-helix-helix transcription factors: variations on a theme. Nat Rev Microbiol. 2007; 5:710–720. [PubMed: 17676053]

Schumacher MA. Bacterial plasmid partition machinery: a minimalist approach to survival. Curr Opin Struct Biol. 2012; 22:72–79. [PubMed: 22153351]

Sergueev K, Dabrazhynetskaya A, Austin S. Plasmid partition system of the P1par family from the pWR100 virulence plasmid of Shigella flexneri. J Bacteriol. 2005; 187:3369–3373. [PubMed: 15866921]

Soding J. Protein homology detection by HMM-HMM comparison. Bioinformatics. 2005; 21:951–960. [PubMed: 15531603]

Stella EJ, Franceschelli JJ, Tasselli SE, Morbidoni HR. Analysis of novel mycobacteriophages indicates the existence of different strategies for phage inheritance in mycobacteria. PLoS One. 2013; 8:e56384. [PubMed: 23468864]

Sternberg N, Austin S. The maintenance of the P1 plasmid prophage. Plasmid. 1981; 5:20–31. [PubMed: 7012872]

Thorvaldsdottir H, Robinson JT, Mesirov JP. Integrative Genomics Viewer (IGV): high-performance genomics data visualization and exploration. Brief Bioinform. 2013; 14:178–192. [PubMed: 22517427]

Villanueva VM, Oldfield LM, Hatfull GF. An Unusual Phage Repressor Encoded by Mycobacteriophage BPs. PLoS One. 2015; 10:e0137187. [PubMed: 26332854]

Wang X, Montero Llopis P, Rudner DZ. Organization and segregation of bacterial chromosomes. Nat Rev Genet. 2013; 14:191–203. [PubMed: 23400100]

Zabala B, Hammerl JA, Espejo RT, Hertwig S. The linear plasmid prophage Vp58.5 of Vibrio parahaemolyticus is closely related to the integrating phage VHML and constitutes a new incompatibility group of telomere phages. J Virol. 2009; 83:9313–9320. [PubMed: 19587034]

Zampini M, Derome A, Bailey SE, Barilla D, Hayes F. Recruitment of the ParG segregation protein to different affinity DNA sites. J Bacteriol. 2009; 191:3832–3841. [PubMed: 19376860]

Zhang H, Gao S, Lercher MJ, Hu S, Chen WH. EvolView, an online tool for visualizing, annotating and managing phylogenetic trees. Nucleic Acids Res. 2012; 40:W569–W572. [PubMed: 22695796]

Zhong L, Cheng Q, Tian X, Zhao L, Qin Z. Characterization of the replication, transfer, and plasmid/lytic phage cycle of the Streptomyces plasmid-phage pZL12. J Bacteriol. 2010; 192:3747–3754. [PubMed: 20472796]

Zhu W, Wang J, Zhu Y, Tang B, Zhang Y, He P, Zhang Y, Liu B, Guo X, Zhao G, Qin J. Identification of three extra-chromosomal replicons in Leptospira pathogenic strain and development of new shuttle vectors. BMC Genomics. 2015; 16:90. [PubMed: 25887950]

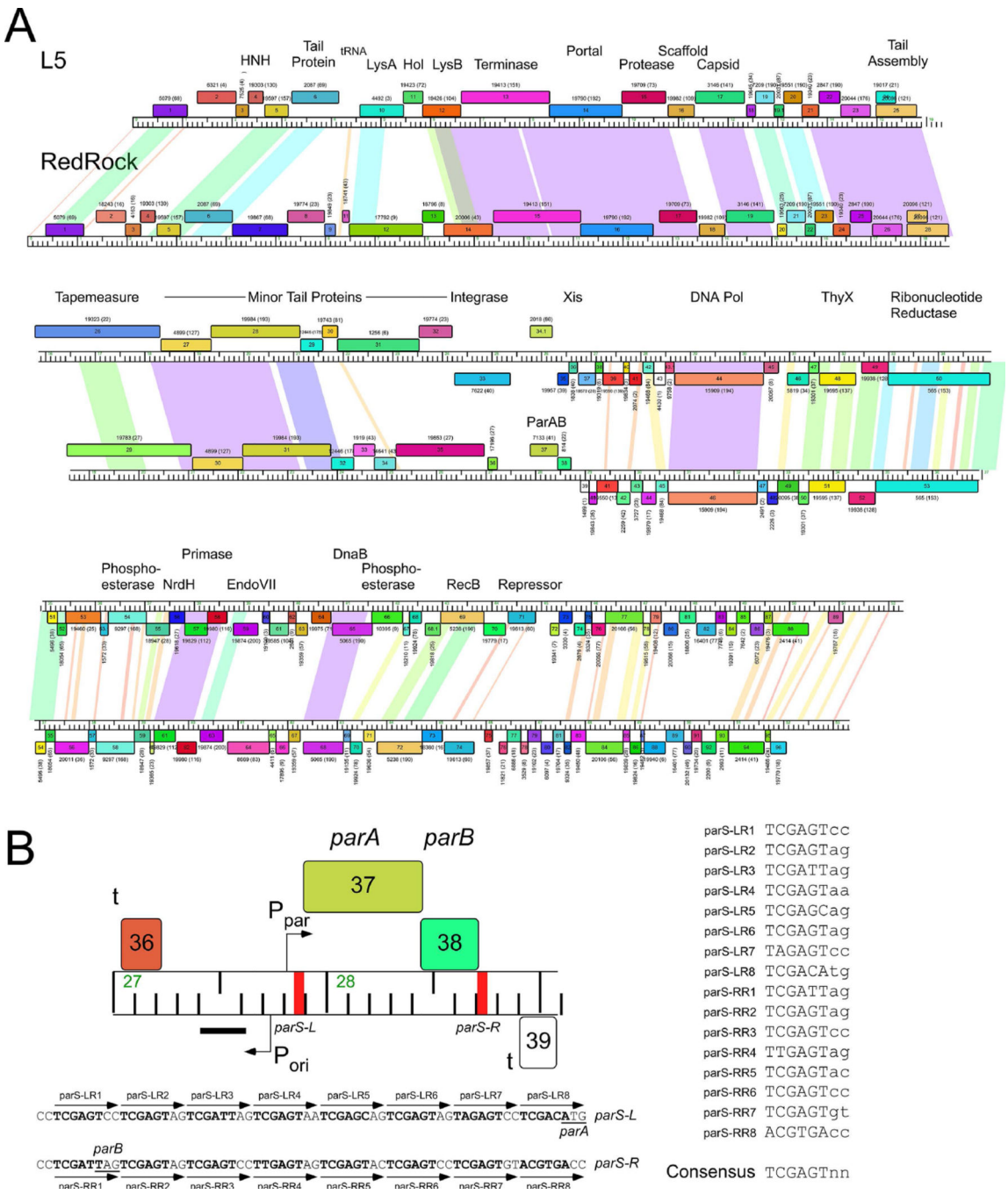

Figure 1.

The *parABS* system of mycobacteriophage RedRock. **A**. Alignment of genome maps of mycobacteriophages RedRock and L5. Both phages are grouped in Subcluster A2 and share similar genomic organizations and sequence similarity. However, at the centers of the genomes L5 contains an integration cassette (*int*, *attP*), whereas RedRock has *parAB* genes. Maps were generated using Phamerator (Cresawn *et al.*, 2011). Predicted genes are shown as boxes transcribed rightwards or leftwards (shown above or below the genome ruler, respectively) with the gene number inside each box. Genes were assorted into phamilies

(phams) of related sequences as described elsewhere (Cresawn *et al.*, 2011, Pope *et al.*, 2015), and colored according to pham membership; pham numbers are shown above or below each gene with the numbers of members in parentheses. Shading between genomes indicates nucleotide sequence similarity determined by BlastN and is spectrum colored with violet being the most similar. **B**. Detailed view of *parABS* organization. The *parAB* genes are transcribed rightwards and are flanked by centromere-like sites *parS-L* and *parS-R*. The location of putative promoters (P) and terminators (t) are shown, as well as a region (black bar) in which a non-coding RNA is highly expressed. Shown below are the sequences for *parS-L* and *parS-R*, with individual 8 bp repeat sequence motifs indicated, which are aligned to provide a consensus sequence on the right.

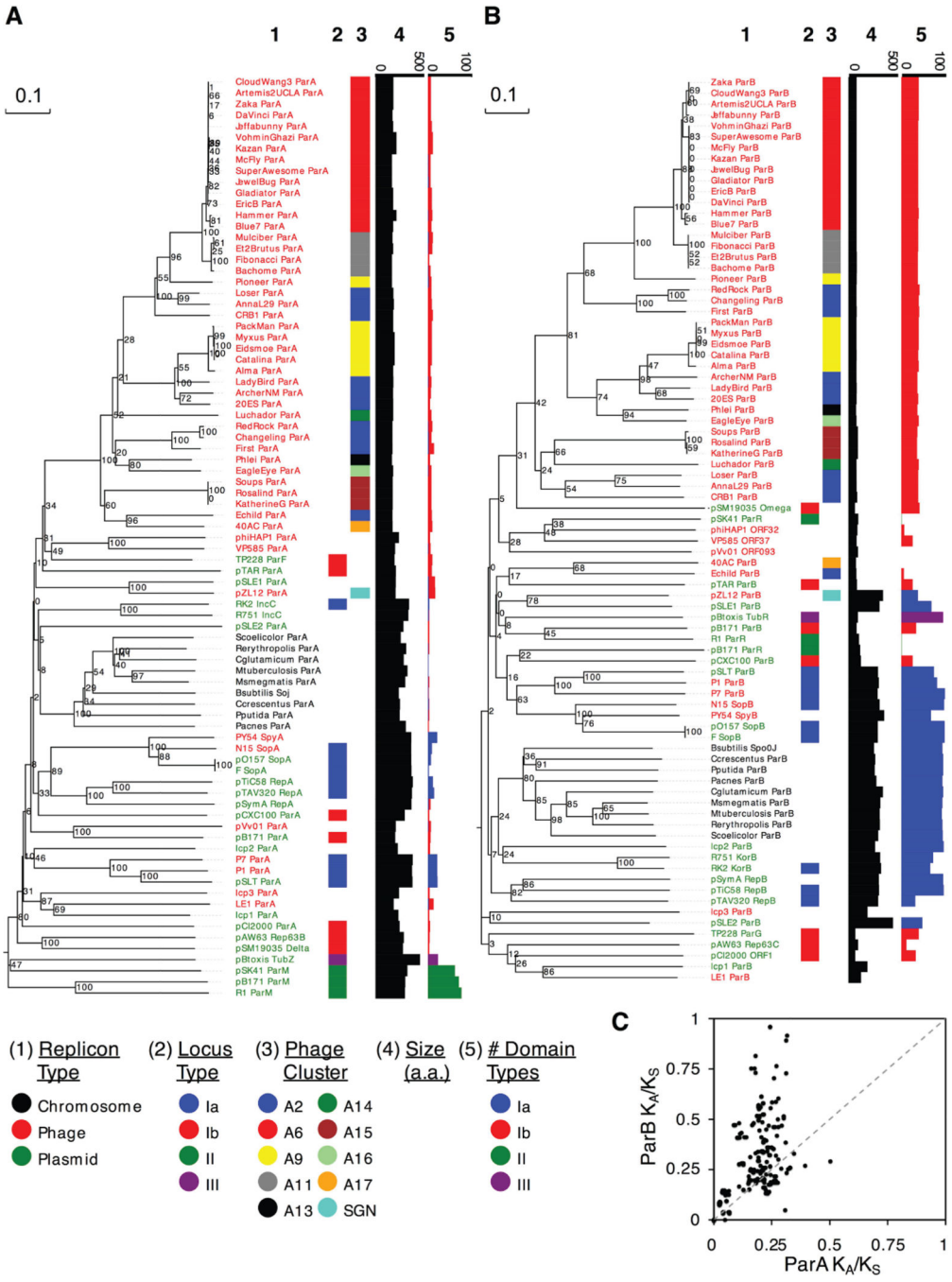

Figure 2.

Phylogenetic comparison of ParA and ParB proteins. Phylogenetic comparison was performed on NTPase ParA-related proteins **(A)** and ParB-like centromere binding proteins **(B)** from 83 characterized and predicted partitioning systems representing different types of partitioning system (Ia, Ib, II, and III) and derived from various types of replicons (chromosomal, plasmid, and phage). Bootstrap values are indicated. For each sequence, the subcluster designation in the Actinobacteriophage_706 database is represented by color (if applicable), the amino acid size is displayed in a horizontal bar graph, and the frequency of

categorized structural domains identified by HHpred analysis is displayed in a colored horizontal bar graph. We note that *Leptospira* lcp1, lcp2, and lcp3 have been predicted to have partitioning cassettes (Zhu *et al.*, 2015), but their roles in segregation have not yet been reported. Although lcp3 ParB has no par type domains and no close relatives, lcp1 ParB groups with LE1 ParB, which has been shown to play a role in plasmid stability (Bourhy *et al.*, 2005), and is positioned in a clade of Type Ib ParBs from TP228, pAW63, and pCI2000 replicons. In contrast, lcp2 is positioned elsewhere in the tree and has many Type Ia domains; likewise, the predicted ParB of the *Streptomyces* plasmids pZL12 (Zhong *et al.*, 2010), pSLE1, and pSLE2 (Gomez-Escribano *et al.*, 2015), also have many Type Ia domains. The cassettes from ΦHAP-1, pVv01 and Vp58.5 (Mobberley *et al.*, 2008, Hammerl *et al.*, 2014, Zabala *et al.*, 2009), exhibit Type Ib similarities, including ParB-like genes adjacent to *parA* that were not previously predicted. **C**. Rate of evolution of ParA and ParB genes. For 27 actinobacteriophages with non-redundant ParA and ParB DNA sequences, a K_A/K_S analysis was performed to compare rates of evolution between the two genes. For all pairwise comparisons of partitioning cassettes, the resulting ParA and ParB K_A/K_S ratios were graphed as a scatter plot. The dotted line reflects how the data would be distributed if both genes experienced similar selective forces.

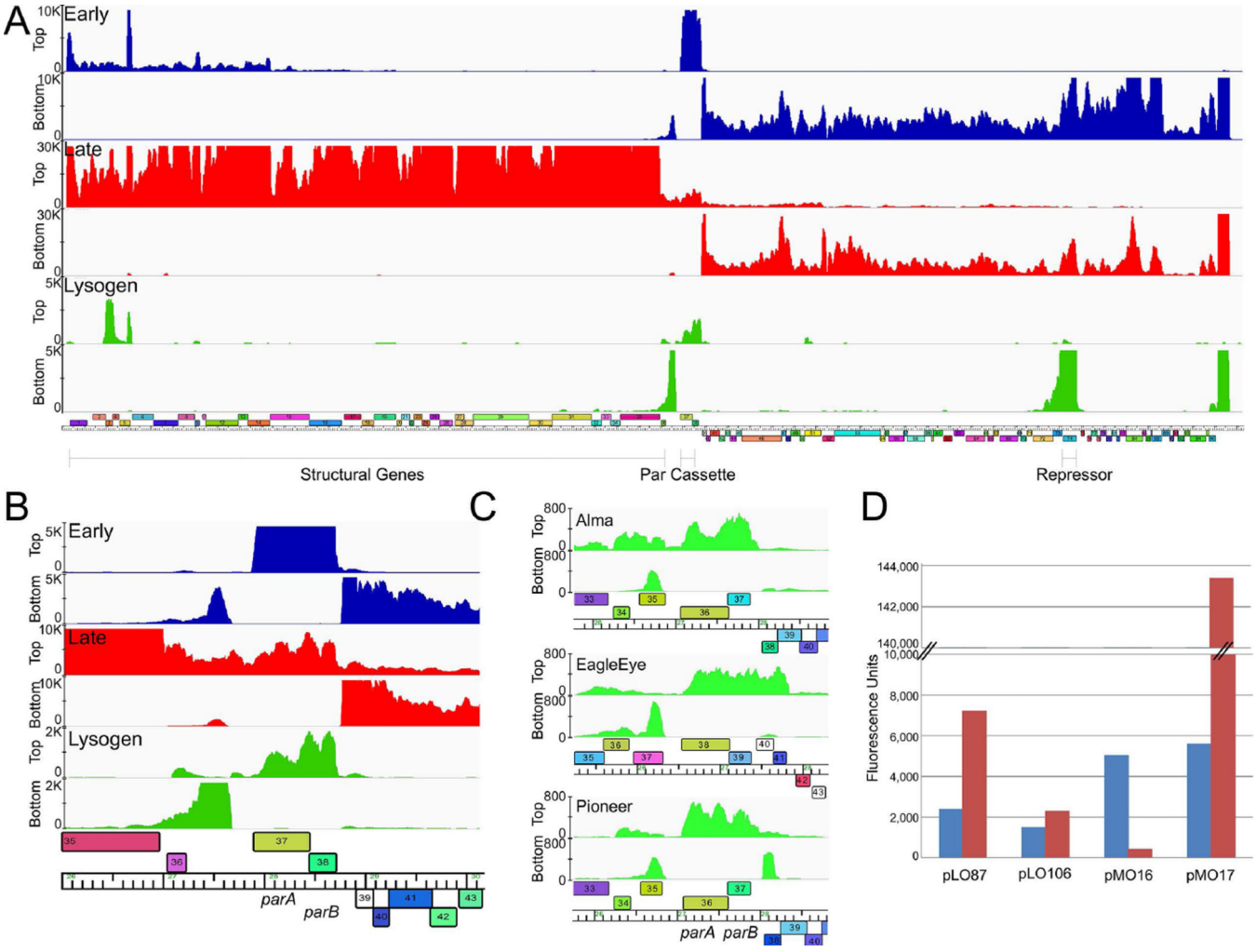

Figure 3.

Expression and regulation of the RedRock *parABS* cassette. **A**. Strand-specific RNAseq analysis of a RedRock lysogen (green) and at early (30 mins; blue) and late (150 mins; red) times post-infection. Lanes corresponding to top and bottom strand sequence reads and scale maxima are shown at the left. A map of the RedRock genome is shown below. **B**. Details of *parAB* expression. Profiles are colored as in panel A. **C**. Detailed view of the RNAseq profiles of the *parAB* genes from Alma, EagleEye, and Pioneer lysogens. The full genome profiles are shown in Fig. S5. **D**. Reporter gene expression of *par*-promoters. The fluorescence of *M. smegmatis* strains containing mCherry reporter plasmids, as indicated, is shown. Strains also lacked (blue bars) or contained (red bars) integrating plasmid pMO15 in which RedRock ParB is expressed from the *hsp60* promoter. Reporter plasmids contain the following promoters: hsp60 (pLO87), phage BPs p6 (pLO106), P_{par} (pMO16), and P_{ori} (pMO17) (see Fig. 1).

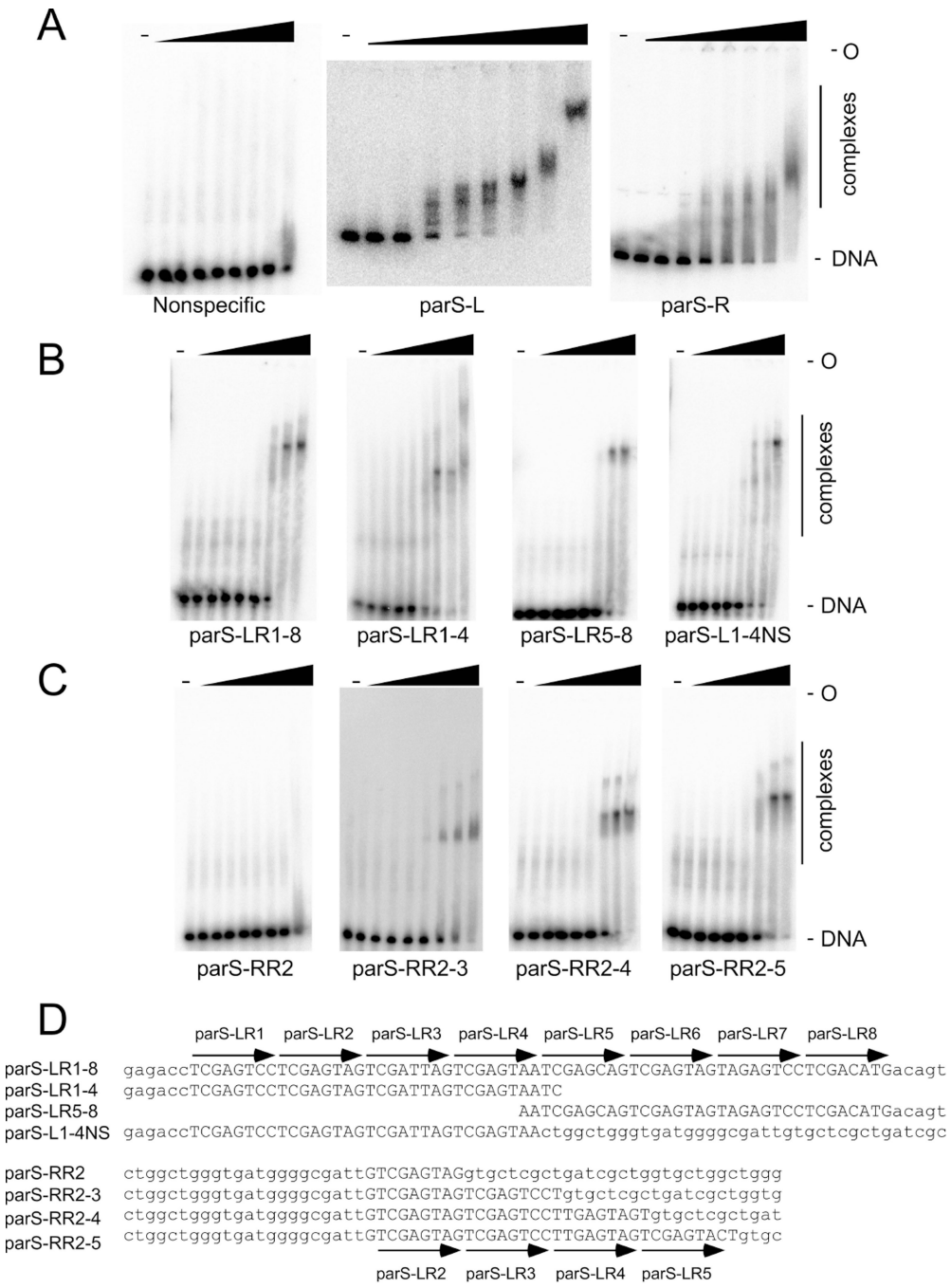

Figure 4.

Binding of RedRock ParB to *parS***A**. Binding of RedRock ParB to *parS-L* and *parS-R*. ParB was incubated at different concentrations to a 45 bp nonspecific DNA fragment (left), a 666 bp fragment containing *parS-L* (middle) and a 194 bp fragment containing *parS-R* (right), and the complexes separated from unbound DNA by native acrylamide gel electrophoresis. Protein concentrations from left to right are : 0, 8.4, 25, 76, 228, 684, 2054, 6163, and 18490 nM. **B**. ParB binding to DNA fragments (from left to right) containing all 8 repeats of *parS-L* (60 bp), the four leftmost repeats (38 bp), the four rightmost repeats (38 bp), and the four

leftmost repeats with flanking nonspecific DNA (60 bp). Protein concentrations are as in panel A. **C**. ParB binding to DNA fragments containing varying numbers of 8 bp repeats. From left to right, increasing the *parS-L* repeat from 1 to 4. Protein concentrations are as in panel A. **D**. The substrates used in panels B and C with the *parS-L* repeats identified.

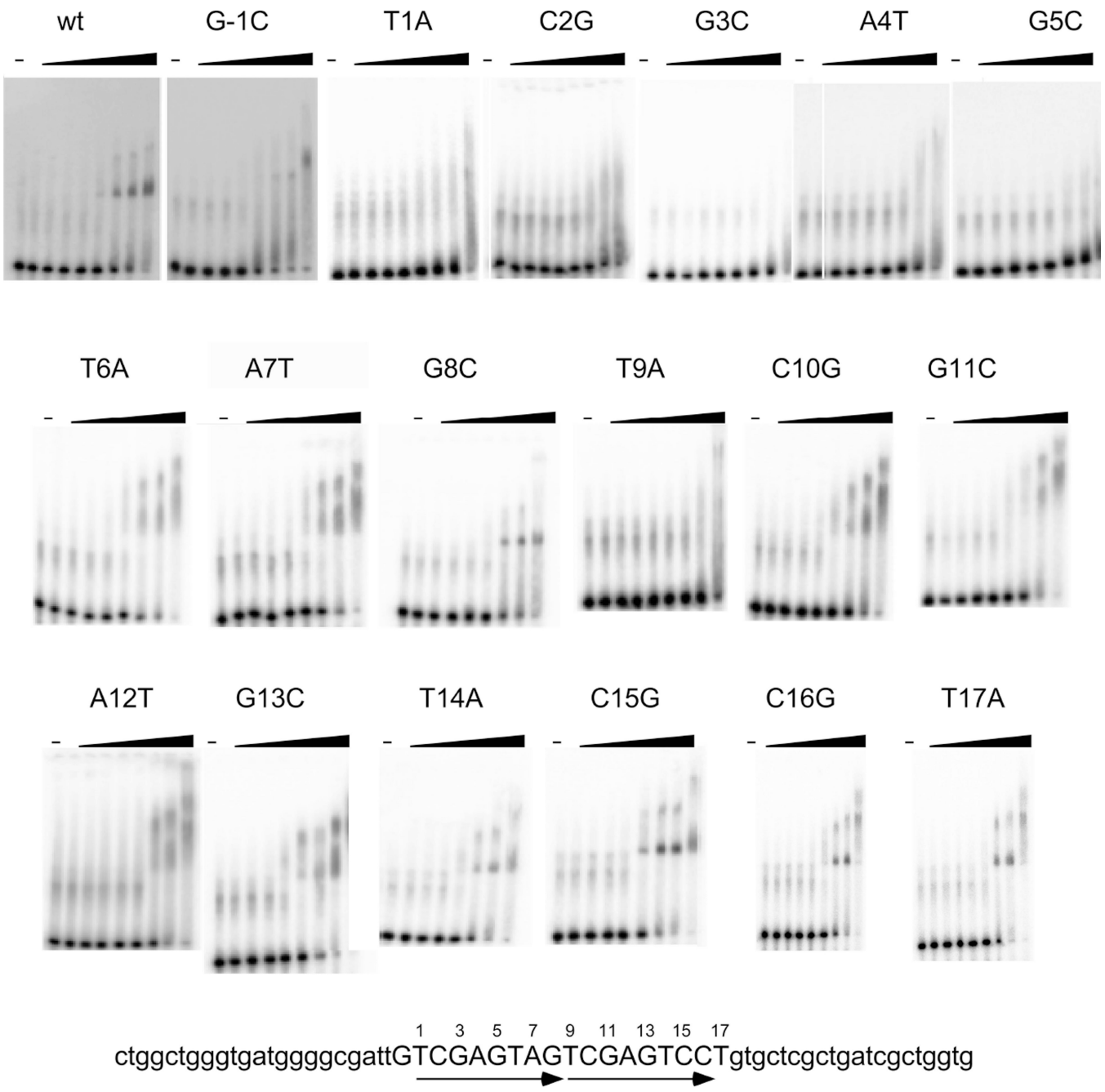

Figure 5.

Mutational analysis of *parS*. The substrate for all EMSAs shown here is at the bottom of the figure. It contains the 18 bp predicted *parS* site and is flanked by nonspecific DNA. This sequence contains two copies of a tandem repeated sequence (shown by arrows). ParB binds to this substrate, but when single base mutations are made and binding is assayed, it is clear that the first repeat sequence is more important for binding. ParB protein concentrations are the same as in Figure 4.

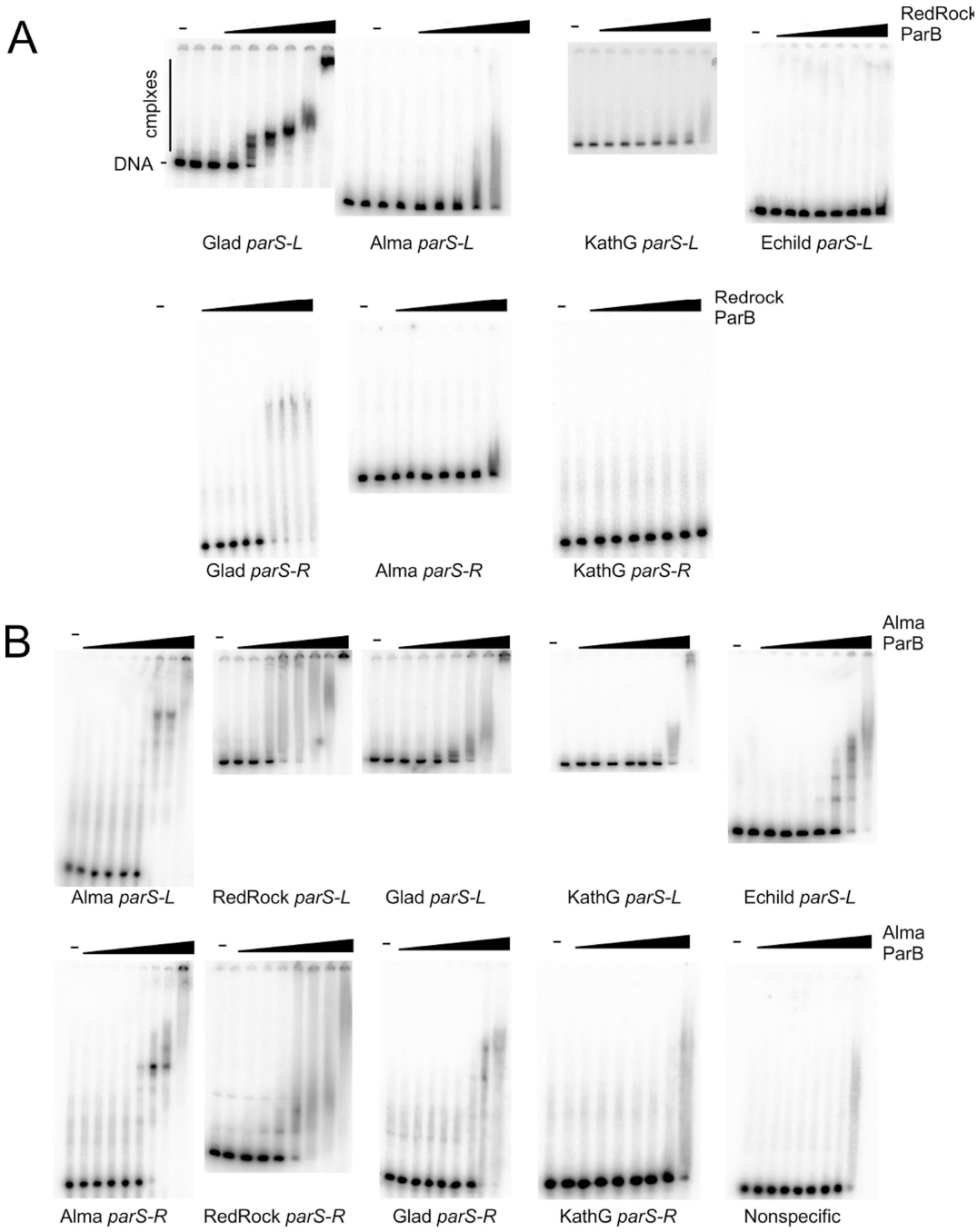

Figure 6.

Specificity of ParB binding to *parS***A**. Binding of RedRock ParB to *parS* sites of mycobacteriophages Alma, Gladiator (Glad), and Echild, as well as Gordonia phage KatherineG (KathG). Gladiator, Alma, and KatherineG, all have predicted *parS-L* and *parS-R* sites flanking the *parAB* genes; a *parS-L* site is predicted upstream of Echild *parA*, but the sequences downstream of Echild *parB* are not obviously related to *parS-R*. Protein concentrations are as in Figure 4, panel A. **B**. Binding of Alma ParB to *parS* sites of mycobacteriophages Alma, RedRock, Gladiator (Glad), and Echild, as well as Gordonia

phage KatherineG (KathG). Protein concentrations of Alma ParB from left to right are: 0, 7.8, 23.4, 70.2, 210, 632, 1896, 5690, and 17070 nM.

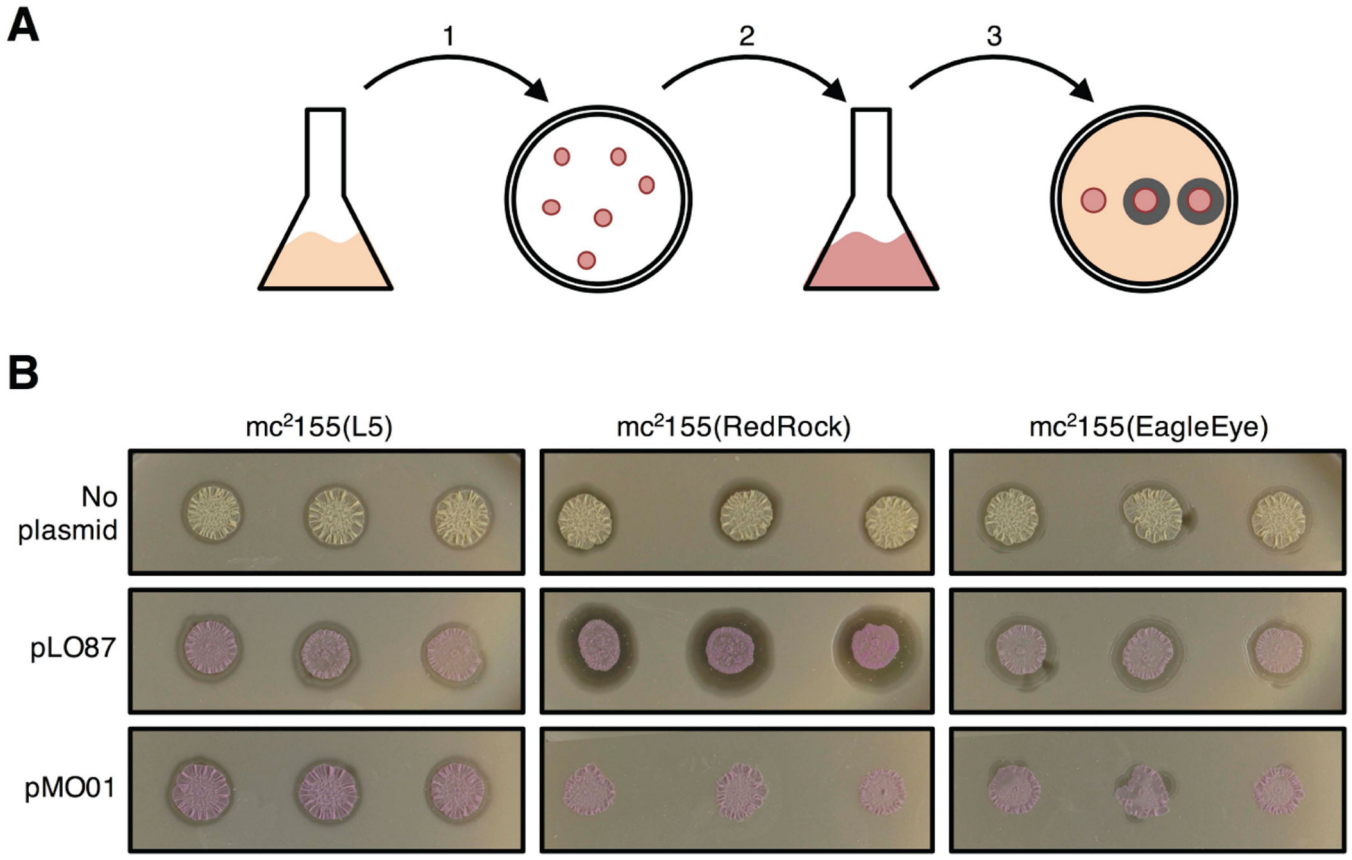

Figure 7.

Phage RedRock *par*-mediated incompatibility. **A**. Scheme to test for *parABS*-mediated incompatibility. Plasmids pMO01 (carrying RedRock *parABS* and *mCherry*), pLO87 (lacking *parABS*) were electroporated into *M. smegmatis* lysogens of L5, RedRock, or EagleEye. and kanamycin-resistant transformants selected (step 1). Three individual red transformants (or un-transformed control colonies) were propagated in liquid selective media (step 2), and spotted onto a lawn of wild type *M. smegmatis* to test for phage release (seen as rings of infection surrounding spotted cultures) indicating lysogeny (step 3). **B**. Plasmid MO01 displaces the RedRock prophage. Three independent transformants carrying pMO01 show no spontaneous phage release indicating prophage loss, which is dependent on *parABS* (pLO87 transformants of RedRock lysogen all show phage release). All transformants and (untransformed cells) of an L5 lysogen show prophage maintenance and compatibility. Spontaneous phage release is reduced in pMO01 transformants of the EagleEye lysogen suggesting partial incompatibility between the RedRock *parABS* in pMO01 and the EagleEye prophage.

Table 1

Whole genome sequence coverage of L5 and RedRock lysogens

	Phage reads[1]	**viral end reads (#)**[2]	***attL*/*attR* reads (#)**	***attP* reads (#)**	**Coverage: Phage**	**Coverage: *M.smegmatis***	**Phage:Host coverage**
mc^{2}155(L5)	41,053	23	141	2	58.9	62.5	0.94
mc^{2}155(RedRock)	105,978	0	N/A	N/A	149	61.8	2.41

[1] Reads mapping to phage genome out of a total of 5.8 million per sample

[2] Reads beginning at precisely the terminus of viral genomic DNA

Table 2

par-mediated plasmid stabilization

Plasmid	Reporter	*par* locus	Plasmid retention (%)[1]
pLO87	*hsp60-mCherry*	None	<1
pMO01	*hsp60-mCherry*	*parSL-parA-parB-parSR*	82[2]
pMO02	*hsp60-mCherry*	*parSL- -parB-parSR*	7
pMO05	*hsp60-mCherry*	*parSL-parA-parB*	71[2]
pMO20	None	None	87[3]
pMO21	None	*parSL-parA-parB-parSR*	100[3]

[1] Plasmid retention determined by percentages of red (pLO87, pMO01, pMO02, pMO05) or kanamycin-resistant (pMO20, pMO21) colonies after 52 generations of unselected growth.

[2] Difference in pMO01 and pMO05 retention levels is not significant (p-value 0.25).

[3] Difference in pMO20 and pMO21 retention is statistically significant (p-value 0.002).